

INVARIANT-DOMAIN PRESERVING IMEX SCHEMES FOR THE NONEQUILIBRIUM GRAY RADIATION-HYDRODYNAMICS EQUATIONS PART I*

JEAN-LUC GUERMOND[†] AND ERIC J. TOVAR^{‡§}

Abstract. In this work we introduce an implicit-explicit invariant-domain preserving approximation of the nonequilibrium gray radiation-hydrodynamics equations. A time and space approximation of the system is proposed using a novel split of the equations composed of three elementary subsystems, two hyperbolic and one parabolic. The approximation thus realized is proved to be consistent, conservative, invariant-domain preserving, and first-order accurate. The proposed method is a stepping stone for achieving higher-order accuracy in space and time in the forthcoming second part of this work. The method is numerically illustrated and shown to converge as advertised. This paper is dedicated to the memory of Peter Lax.

Key words. Radiation hydrodynamics, nonequilibrium gray diffusion, invariant domain preserving, IMEX, Euler equations

AMS subject classifications. 35L65, 65M60, 65M12, 65N30

1. Introduction. The objective of this work is to introduce a first-order approximation of the nonequilibrium gray radiation hydrodynamics (GRH) equations that is invariant-domain preserving (IDP), consistent, and conservative. The GRH equations play an important role in modeling the diffusion of thermal radiation in fluids as well as the induced effects of radiation on the fluid motion. The model is typically used for applications in optically thick environments (i.e., strong coupling between radiation and fluid motion) such as inertial confinement fusion and astrophysics (see: Baldwin et al. [2]). The GRH equations is a system composed of the compressible Euler equations coupled to a parabolic equation for the radiation energy density where both sub-systems are supplemented with stiff source terms. We refer the reader to Mihalas and Mihalas [31, Sec. 97] for a general overview of the model and Buet and Despres [5] where a formal derivation of the model is presented.

Due to the disparate temporal scales of the radiation and fluid motion, developing robust and accurate approximation techniques for the model is challenging. It is known that applying an explicit time-integration method to the model leads to a restrictive time-step, $\Delta t \sim \frac{\sigma_t \times (\Delta x)^2}{c}$, where c is the speed of light, σ_t is the total absorption opacity, and Δx is the spatial mesh size (see: Baldwin et al. [2]). Alternatively, one could apply implicit time-integration to the full system but this could be computationally burdensome. A natural approach for overcoming these challenges

[†]Department of Mathematics, Texas A&M University 3368 TAMU, College Station, TX 77843, USA.

[‡]Theoretical Division, Los Alamos National Laboratory, P.O. Box 1663, Los Alamos, NM, 87545, USA.

[§]Xcimer Energy Corporation, 10325 E 47th Ave, Denver, CO, 80238, USA.

*This material is based upon work supported in part by the National Science Foundation grant DMS2110868, the Air Force Office of Scientific Research, USAF, under grant/contract number FA9550-23-1-0007, and the U.S. Department of Energy by Lawrence Livermore National Laboratory under Contracts B640889. ET acknowledges the former support from the U.S. Department of Energy's Office of Applied Scientific Computing Research (ASCR) through the Competitive Portfolios program at Los Alamos National Laboratory (LANL). LANL is operated by Triad National Security, LLC, for the National Nuclear Security Administration of the U.S. Department of Energy (Contract No. 89233218CNA000001). The LANL release number is LA-UR-26-20761. The support of Xcimer Energy Corporation is also acknowledged.

would be to apply operator splitting to the system and use an IMEX time-integration method. Some recent approaches in the literature following this idea can be seen in Bolding et al. [4] and Southworth et al. [36]. An operator split method was applied to the equilibrium diffusion model in Dai and Woodward [10]. Another challenge in developing robust numerical methods for the GRH model is the stiff non-linearity that arises in the radiation diffusion sub-system due to potentially highly contrasted opacities (which depend on density and temperature). Efforts in the literature addressing this issue can be seen in Baldwin et al. [2] and Knoll et al. [23] for the radiation diffusion sub-system. For papers regarding only the radiation diffusion sub-system with a focus on time integration techniques, we refer the reader to Knoll et al. [24] and Zheng et al. [38]. For papers regarding positivity of the solution for the radiation diffusion sub-system and positivity see Buet and Despres [6] and Sheng et al. [35]. Recent work on developing higher-order approximation techniques for the full GRH model can be seen in Delchini et al. [12] and Delchini et al. [13]. Since the nonequilibrium GRH diffusion model is a simplified radiation-hydrodynamics model, we refer the reader to Bolding et al. [4] and He et al. [22] for higher-order IMEX schemes applied to generalized radiation-hydrodynamic models. The literature addressing positivity preservation, or more generally, invariant-domain preservation is sparse. The purpose of the present paper is to address this issue.

The contribution of this work is as follows. We introduce a novel split of the GRH model into two elementary hyperbolic systems and one parabolic system. The motivation for introducing two hyperbolic stages is rooted in the observation that the radiation pressure does not influence the material internal energy; see e.g., Lemma 2.4 in Dao et al. [11]. To the authors' best knowledge, this split seems to be original. Furthermore, using [17], this split allows for a straight-forward spatial approximation that is invariant-domain preserving for each hyperbolic system. We also derive the maximum wave speed in the local Riemann problem for the second hyperbolic system to guarantee the IDP property. Then, we introduce a simple approximation to the parabolic sub-system using backward Euler time stepping. This approximation utilizes a fixed-point Picard iteration method and a local Newton solve for updating the radiation energy density and material temperature. The fixed-point technique is used to ensure robustness of the algorithm at high Mach numbers. Finally, irrespective of the relative tolerance that is used to exit the fixed-point loop, the approximation is shown to be invariant-domain preserving under mild assumptions on the equation of state and the underlying spatial approximation.

The paper is organized as follows. In Section 2 we recall the full nonequilibrium gray radiation hydrodynamics (GRH) model and discuss its properties. We also give a brief background on the thermodynamics and invariant domain of the system. In Section 3, we introduce a novel split of the GRH model which is composed of two hyperbolic subsystems and one parabolic subsystem. Then, in Section 4 we discuss details regarding the spatial approximation and list some structural assumptions that are invoked later. Section 5 is dedicated to the approximation technique of the full system. We focus on the approximation of the two hyperbolic problems in Sections 5.1 and 5.2. We give a brief discussion on multiplicative vs. additive splitting in Section 5.3. The main results of these sections are Lemmas 5.1 and 5.3. We discuss the approximation to the parabolic stage in Section 5.4. We detail the fixed-point Picard iteration and the Newton method in this section. The main result of this section is Lemma 5.5 and the main result of the paper is stated in Theorem 5.6. Finally, we conclude by numerically illustrating the proposed approximation technique.

2. The model. In this section, we introduce the model for nonequilibrium gray radiation hydrodynamics. We then give a brief discussion on the respective thermodynamics and invariant domain properties.

2.1. Governing equations. Let D be a domain in \mathbb{R}^d where $d = \{1, 2, 3\}$. Assume that the domain is occupied by a radiating fluid that is optically thick. That is to say, the gradient of the radiation energy density varies slowly over the photon mean-free path (Bates et al. [3]). This assumption implies that the fluid motion and radiation are strongly coupled. We assume that the opacity of the material is independent of the frequency of photons in the radiation, i.e., the fluid is a “gray” material (Lowrie et al. [29]). We further assume that the fluid and radiation fields are not in thermodynamic equilibrium. The nonequilibrium gray radiation hydrodynamics diffusion model corresponding to this situation is written as follows:

$$\begin{aligned} (2.1a) \quad & \partial_t \rho + \nabla \cdot (\mathbf{v} \rho) = 0, \\ (2.1b) \quad & \partial_t \mathbf{m} + \nabla \cdot (\mathbf{v} \otimes \mathbf{m} + p(\mathbf{u}) \mathbb{I}_d) + \nabla p_r(\mathbf{u}) = \mathbf{0}, \\ (2.1c) \quad & \partial_t E_m + \nabla \cdot (\mathbf{v}(E_m + p(\mathbf{u}))) + \mathbf{v} \cdot \nabla p_r(\mathbf{u}) = -\sigma_a c (a_r T(\mathbf{u})^4 - E_r), \\ (2.1d) \quad & \partial_t E_r + \nabla \cdot (\mathbf{v} E_r) + p_r(\mathbf{u}) \nabla \cdot \mathbf{v} - \nabla \cdot \left(\frac{c}{3\sigma_t} \nabla E_r \right) = \sigma_a c (a_r T(\mathbf{u})^4 - E_r). \end{aligned}$$

Here, the (column) vector of the conserved variables has $d + 3$ components $\mathbf{u} := (\rho, \mathbf{m}^\top, E_m, E_r)^\top$, where ρ is the density, \mathbf{m} is the momentum (viewed as a column vector in \mathbb{R}^d), E_m is the total mechanical energy, and E_r is the radiation energy (per unit volume). We define the velocity vector by $\mathbf{v} := \rho^{-1} \mathbf{m}$. Here $p_r(\mathbf{u})$ is the radiation pressure, c the speed of light, σ_a and σ_t the absorption and total cross sections (both scale as the inverse of a length), respectively, $a_r := \frac{4\sigma}{c}$ the radiation constant, σ the Stefan–Boltzmann constant, and $p(\mathbf{u})$, $T(\mathbf{u})$ are the mechanical pressure and temperature, respectively. More details regarding $p(\mathbf{u})$ and $T(\mathbf{u})$ are given in §2.2. We also define the internal energy $\varepsilon(\mathbf{u}) := E_m - \frac{1}{2} \rho \|\mathbf{v}\|_{\ell^2}^2$, the specific internal energy $e(\mathbf{u}) := \rho^{-1} \varepsilon(\mathbf{u}) := \rho^{-1} E_m - \frac{1}{2} \|\mathbf{v}\|_{\ell^2}^2$, and the total energy of the system by $E_{\text{tot}} := E_m + E_r$. For the rest of the paper, we assume that the radiation pressure is defined by $p_r(\mathbf{u}) := \frac{1}{3} E_r$. We refer the reader to §6.1 for a discussion on the units used in this work.

Remark 2.1 (Total energy). Adding (2.1c) and (2.1d), we observe that the total energy of the system satisfies the balance equation:

$$(2.2) \quad \partial_t E_{\text{tot}} + \nabla \cdot (\mathbf{v}(E_{\text{tot}} + p(\mathbf{u}) + p_r(\mathbf{u}))) - \nabla \cdot \left(\frac{c}{3\sigma_t} \nabla E_r \right) = 0,$$

which shows that, in absence of energy source fluxes at the boundary of the domain D , the total energy is conserved, as expected. The three conserved variables of the system are the density, ρ , the momentum, \mathbf{m} , and the total energy, E_{tot} . The radiation energy is not a conserved quantity. \square

Remark 2.2 (Internal energy). Taking the dot product of (2.1b) with \mathbf{v} and subtracting the result from (2.1c) gives the balance equation for the internal energy:

$$(2.3) \quad \partial_t (\rho e(\mathbf{u})) + \nabla \cdot (\mathbf{v} \rho e(\mathbf{u})) + p(\mathbf{u}) \nabla \cdot \mathbf{v} = -\sigma_a c (a_r T(\mathbf{u})^4 - E_r),$$

which shows that the gradient of the radiation pressure has no effect whatsoever on the internal energy. We refer the reader to Lemma 2.4 in Dao et al. [11] where a more general statement regarding this property is made. \square

Remark 2.3 (Nonconservative products). Notice that (2.1) has non-conservative products $\mathbf{v} \cdot \nabla p_r(\mathbf{u})$ and $p_r(\mathbf{u}) \nabla \cdot \mathbf{v}$. However, due to the presence of the diffusive term $\nabla \cdot (\frac{c}{3\sigma_t} \nabla E_r)$ in (2.1d), it is reasonable to expect that no discontinuity appears in the variable E_r so that these non-conservative product are unambiguously defined. The reader is also referred to Buet and Despres [6, §2.4] where the non-conservative product question is discussed. \square

Remark 2.4 (Thermodynamic nonequilibrium). In the literature, the term *equilibrium* refers to the case when the radiation energy density and material temperature satisfy the condition $E_r = a_r T(\mathbf{u})^4$ for all $\mathbf{x} \in D$ and all $t > 0$. For a thorough discussion of the equilibrium-diffusion limit of the radiation hydrodynamics equations, we refer the reader to Dai and Woodward [10] and Ferguson et al. [15] and references therein. \square

2.2. Thermodynamics and invariant domain. Throughout the paper, we assume that given a reasonable state \mathbf{u} , we are able to retrieve the mechanical pressure $p(\mathbf{u})$ and temperature $T(\mathbf{u})$ in a suitable way (e.g., by evaluating arbitrary analytic expressions or by deriving values from tabulated experimental data). We call the equation of state that relates these thermodynamic quantities, the oracle. We assume that we have no a priori knowledge of the oracle apart from some mild structural assumptions that we now state. As in Clayton et al. [9], we assume that the domain of definition for the thermodynamic quantities is the set $\mathcal{B}(b) \subset \mathbb{R}^{d+3}$ given by

$$(2.4) \quad \mathcal{B}(b) := \{ \mathbf{u} := (\rho, \mathbf{m}^\top, E_m, E_r)^\top \in \mathbb{R}^{d+3} \mid 0 < \rho, 0 < 1 - b\rho, e_{\text{cold}}(\rho) < e(\mathbf{u}) \}.$$

The inequality $1 - b\rho > 0$ appearing in the definition of $\mathcal{B}(b)$ is the so called maximum compressibility condition. The constant b can be set to zero if the user has no a priori knowledge about the maximum compressibility of the fluid under consideration. The function $e_{\text{cold}} : \mathbb{R}_{>0} \rightarrow \mathbb{R}$ is the cold curve. We henceforth assume that $e_{\text{cold}} : (0, \frac{1}{b}) \rightarrow \mathbb{R}$ is quasiconcave. For the sake of simplicity, we assume that the oracle returns a pressure and a non-negative temperature:

$$(2.5) \quad p : \mathcal{B}(b) \ni \mathbf{u} \longmapsto p(\mathbf{u}) \in \mathbb{R},$$

$$(2.6) \quad T : \mathcal{B}(b) \ni \mathbf{u} \longmapsto T(\mathbf{u}) \in \mathbb{R}_{\geq 0}.$$

The temperature being positive is one of the fundamental principles of thermodynamics. Recall that using the definition of the heat capacity at constant volume $\mathfrak{c}_v(\rho, T) := \frac{\partial e}{\partial T}(\rho, T) > 0$, we have $e(\rho, T) = \int_0^T \mathfrak{c}_v(\rho, \theta) d\theta + e_{\text{cold}}(\rho)$. Then, again for the sake of simplicity, we assume that the oracle gives us access to the cold curve $e_{\text{cold}}(\rho)$ and the average heat capacity at constant volume $c_v(\rho, T) := \frac{1}{T} \int_0^T \mathfrak{c}_v(\rho, \theta) d\theta$. We summarize this assumption by saying that the internal energy and the temperature are related as follows:

$$(2.7) \quad e(\mathbf{u}) = c_v(\rho, T(\mathbf{u})) T(\mathbf{u}) + e_{\text{cold}}(\rho), \quad \forall \mathbf{u} \in \mathcal{B}(b).$$

We note that the above assumptions can be weakened. The reader is referred to Clayton and Tovar [7] for more details on how to weaken these assumptions, but these generalizations are out of the scope of the paper.

Regarding the radiation quantities, we assume that the absorption and total cross sections can depend on the oracle; that is to say, we assume the following properties for the absorption and total cross sections $\sigma_a : \mathcal{B}(b) \ni \mathbf{u} \longmapsto \sigma_a(\rho, T(\mathbf{u})) \in \mathbb{R}_{\geq 0}$ and $\sigma_t : \mathcal{B}(b) \ni \mathbf{u} \longmapsto \sigma_t(\rho, T(\mathbf{u})) \in \mathbb{R}_{>0}$.

Since it can be shown that the following set

$$(2.8) \quad \mathcal{A}(b) := \{\mathbf{u} = (\rho, \mathbf{m}^\top, E_m, E_r)^\top \in \mathbb{R}^{d+3} \mid 0 < \rho, 0 < 1 - b\rho, e_{\text{cold}}(\rho) < e(\mathbf{u}), 0 < E_r\}$$

is invariant under parabolic regularization, we focus our interest only on those weak solutions of (2.1) for which $\mathcal{A}(b)$ is invariant as well. Our ultimate objective is to construct an approximation of (2.1) that is high-order accurate in space and time and leaves $\mathcal{A}(b)$ invariant. We propose to do so by first constructing a first-order method that is IDP, then constructing a higher-order method that is made IDP by limiting. The objective of the present paper is to solely focus on the first-order IDP method.

3. Three elementary subsystems. In this section, we introduce the novel split of the model (2.1). This split consists of three elementary subsystems (two hyperbolic and one parabolic). The purpose of this section is simply to give the reader some heuristics justifying the decomposition of the system that is used in §5 to perform the approximation in time.

3.1. IMEX split (hyperbolic-parabolic). The approximation in time of (2.1) is done by means of an implicit-explicit (IMEX) time stepping technique. The explicit time stepping is applied to the non-stiff part of the problem:

$$\begin{aligned} (3.1a) \quad & \partial_t \rho + \nabla \cdot (\mathbf{v} \rho) = 0, \\ (3.1b) \quad & \partial_t \mathbf{m} + \nabla \cdot (\mathbf{v} \otimes \mathbf{m} + p(\mathbf{u}) \mathbb{I}_d) = -\nabla p_r(\mathbf{u}), \\ (3.1c) \quad & \partial_t E_m + \nabla \cdot (\mathbf{v} (E_m + p(\mathbf{u}))) = -\mathbf{v} \cdot \nabla p_r(\mathbf{u}), \\ (3.1d) \quad & \partial_t E_r + \nabla \cdot (\mathbf{v} E_r) = -p_r(\mathbf{u}) \nabla \cdot \mathbf{v}, \end{aligned}$$

whereas the implicit time stepping is applied of the stiff part:

$$\begin{aligned} (3.2a) \quad & \partial_t \rho = 0, \\ (3.2b) \quad & \partial_t \mathbf{m} = \mathbf{0}, \\ (3.2c) \quad & \partial_t E_m = -\sigma_a c (a_r T(\mathbf{u})^4 - E_r), \\ (3.2d) \quad & \partial_t E_r - \nabla \cdot (\frac{c}{3\sigma_t} \nabla E_r) = \sigma_a c (a_r T(\mathbf{u})^4 - E_r). \end{aligned}$$

We henceforth refer to (3.1) as the hyperbolic sub-problem (or stage) and we refer to (3.2) as the parabolic sub-problem (or stage).

To be able to construct an approximation method that is consistent, conservative, and leaves $\mathcal{A}(b)$ invariant, we further decompose (3.1). The decomposition is based on the observation that the radiation pressure does not have any influence on the internal energy, as stated in Remark 2.2. We split (3.1) into two stages to account for this fundamental principle.

3.1.1. Hyperbolic stage 1. In the first stage of the solution process for (3.1), which we henceforth call hyperbolic stage 1, we just account for the influence of the mechanical pressure $p(\mathbf{u})$ in the time evolution of the momentum and mechanical total energy. The effect of the radiation pressure is accounted for in the second stage. The first stage is formulated as follows: Given some initial data $(\rho_0, \mathbf{m}_0^\top, E_{m0}, E_{r0})^\top$, find $\mathbf{u} := (\rho, \mathbf{m}^\top, E_m, E_r)^\top$ s.t.

$$(3.3) \quad \partial_t \mathbf{u} + \nabla \cdot \mathbf{g}(\mathbf{u}) = \mathbf{0}, \quad \text{with} \quad \mathbf{g}(\mathbf{u}) := \begin{pmatrix} \mathbf{v} \rho \\ \mathbf{v} \otimes \mathbf{m} + p(\mathbf{u}) \mathbb{I}_d \\ \mathbf{v} (E_m + p(\mathbf{u})) \\ \mathbf{v} E_r \end{pmatrix}.$$

This system is just the compressible Euler equation augmented with an additional linear conservation equation for the radiation energy. Approximating this problem in time and space is a standard exercise explained in §5.1.

3.1.2. Hyperbolic stage 2. The second stage, which we henceforth call hyperbolic stage 2, reads as follows: Given some initial data $(\rho_0, \mathbf{m}_0^\top, E_{m0}, E_{r0})^\top$, seek $(\rho, \mathbf{m}^\top, E_m, E_r)^\top$ so that

$$(3.4a) \quad \partial_t \rho = 0,$$

$$(3.4b) \quad \partial_t \mathbf{m} = -\nabla p_r(E_r),$$

$$(3.4c) \quad \partial_t E_m = -\mathbf{v} \nabla p_r(E_r),$$

$$(3.4d) \quad \partial_t E_r = -p_r(E_r) \nabla \cdot \mathbf{v}.$$

It turns out that the system (3.4) can be further simplified and be put in conservative form. Notice that (3.4b) combined with (3.4c) implies that the internal energy, $\varepsilon(\mathbf{u}) := \rho e(\mathbf{u}) := E_m - \frac{1}{2} \rho \|\mathbf{v}\|_{\ell^2}^2$, is constant in time (in agreement with the statement already made in Remark 2.2, see [11, Lem 2.4]). Likewise, combining (3.4b) and (3.4d), we obtain a conservation equation for the quantity $E_t := E_r + \frac{1}{2} \rho \|\mathbf{v}\|_{\ell^2}^2$ (not to be confused with E_{tot}). In conclusion, (3.4) can be rewritten in the following equivalent form:

$$(3.5a) \quad \partial_t \rho = 0,$$

$$(3.5b) \quad \partial_t \mathbf{m} = -\nabla p_r(E_r),$$

$$(3.5c) \quad \partial_t E_t = -\nabla \cdot (\mathbf{v} p_r(E_r)),$$

$$(3.5d) \quad \partial_t \varepsilon(\mathbf{u}) = 0.$$

Hence, given the initial data $(\rho_0, \mathbf{m}_0^\top, E_{m0}, E_{r0})^\top$, setting $E_{t0} := E_{r0} + \frac{1}{2} \rho_0 \|\mathbf{v}_0\|_{\ell^2}^2$, seek we $\mathbf{w} := (\rho, \mathbf{m}^\top, E_t)^\top$ such that

$$(3.6) \quad \partial_t \mathbf{w} + \nabla \cdot \mathbf{k}(\mathbf{u}) = \mathbf{0}, \quad \mathbf{k}(\mathbf{w}) := \begin{pmatrix} 0 \\ p_r(\mathbf{w}) \mathbb{I}_d \\ \mathbf{v} p_r(\mathbf{w}) \end{pmatrix}, \quad p_r(\mathbf{w}) := \frac{1}{3} (E_t - \frac{1}{2} \rho \|\mathbf{v}\|_{\ell^2}^2),$$

and $\partial_t \varepsilon(\mathbf{u}) = 0$. After solving (3.6) and setting $\varepsilon_0 := E_{m0} - \frac{1}{2} \rho_0 \|\mathbf{v}_0\|_{\ell^2}^2$, the full state $(\rho, \mathbf{m}^\top, E_m, E_r)^\top$ is recovered by setting

$$(3.7) \quad E_r := E_t - \frac{1}{2} \rho \|\mathbf{v}\|_{\ell^2}^2, \quad E_m := \varepsilon_0 + \frac{1}{2} \rho \|\mathbf{v}\|_{\ell^2}^2 = E_{m0} - \frac{1}{2} \rho_0 \|\mathbf{v}_0\|_{\ell^2}^2 + \frac{1}{2} \rho \|\mathbf{v}\|_{\ell^2}^2.$$

3.1.3. Parabolic stage. Finally, the third stage of the decomposition of the system (2.1) consists of rewriting the parabolic stage (3.2) as follows: Given some initial data $(\rho_0, \mathbf{m}_0^\top, E_{m0}, E_{r0})^\top$, set $\mathbf{v}_0 := \mathbf{m}_0 / \rho_0$, $e_0 := \rho_0^{-1} (E_{m0} - \frac{1}{2} \|\mathbf{v}_0\|_{\ell^2}^2)$, and $T_0 := T(\rho_0, e_0)$, then seek $(\rho, \mathbf{v}^\top, T, E_r)^\top$ such that

$$(3.8a) \quad \partial_t \rho = 0,$$

$$(3.8b) \quad \partial_t \mathbf{v} = \mathbf{0},$$

$$(3.8c) \quad \rho \partial_t (c_v T) = -\sigma_a c (a_r T^4 - E_r),$$

$$(3.8d) \quad \partial_t E_r - \nabla \cdot \left(\frac{c}{3\sigma_a} \nabla E_r \right) = \sigma_a c (a_r T^4 - E_r),$$

where we used the fact that $\partial_t e = c_v \partial_t T$ in (3.8c). We recover the internal energy after solving (3.8) by setting $e = c_v T$, which finally give $E_m := \rho e + \frac{1}{2} \rho \|\mathbf{v}\|_{\ell^2}^2$.

The three elementary problems (3.3), (3.6), and (3.8) are going to play important roles when we prove that our, yet to be constructed, low-order method is conservative and invariant-domain preserving.

4. Approximation details. Although the numerical tests reported in the paper are done with continuous finite elements, most of what is said herein is independent of the spatial discretization. Up to unessential adaptations, all the theoretical results established below hold for finite differences, finite volumes, continuous and discontinuous finite elements.

Assumption 4.1. To make the presentation of the method discretization agnostic, we make the following assumptions (i)–(v):

(i) The space approximation of any state functions $\mathbf{u} : D \rightarrow \mathbb{R}^{d+3}$ is entirely defined by a finite collection of states $\mathbf{u} := \{\mathbf{u}_i\}_{i \in \mathcal{V}}$, where the coefficients \mathbf{u}_i (henceforth called degrees of freedom) are \mathbb{R}^{d+3} -valued, $\mathcal{V} := \{1:I\}$ is the index set enumerating the degrees of freedom, and we have set $I := \text{card}(\mathcal{V})$. We also assume that \mathcal{V} is partitioned into interior degrees of freedom, \mathcal{V}° , and boundary degrees of freedom \mathcal{V}^∂ , i.e., $\mathcal{V} := \mathcal{V}^\circ \cup \mathcal{V}^\partial$ and $\mathcal{V}^\circ \cap \mathcal{V}^\partial = \emptyset$. For instance, if the approximation is done with finite elements using global shape function $\{\varphi_i\}_{i \in \mathcal{V}}$ and $\mathbf{u}_h = \sum_{i \in \mathcal{V}} \mathbf{u}_i \varphi_i$ is the approximation of some function \mathbf{u} , then the only information that is relevant to us regarding the approximate function \mathbf{u}_h is the collection $\{\mathbf{u}_i\}_{i \in \mathcal{V}}$. Interior degrees of freedom for Lagrange elements are such that $\varphi_{i|\partial D} = 0$ for all $i \in \mathcal{V}^\circ$.

(ii) For every $i \in \mathcal{V}$, there exists a subset $\mathcal{V}(i) \subsetneq \mathcal{V}$ that collects the local degrees of freedom that interact with i , which we call stencil at i . We assume that $j \in \mathcal{V}(j)$ iff $i \in \mathcal{V}(j)$. We denote $\mathcal{V}^*(i) := \mathcal{V}(i) \setminus \{i\}$.

(iii) The underlying spatial discretization provides two $I \times I$ real-valued matrices \mathbb{M}^L and \mathbb{M}^H with the following properties. \mathbb{M}^L is invertible, diagonal, and is called low-order mass matrix. The entries of this matrix are denoted $\mathbb{M}_{ij}^L = m_i \delta_{ij}$ where m_i is called the mass associated with the i -th degree of freedom. \mathbb{M}^H is invertible, symmetric, and is called high-order mass matrix. The entries of this matrix are denoted $\mathbb{M}_{ij}^H = m_{ij}$ and are assumed to be such that $m_{ij} = 0$ if $j \notin \mathcal{V}(i)$, i.e., $(\mathbb{M}^H \mathbf{X})_i = \sum_{j \in \mathcal{V}(i)} m_{ij} \mathbf{X}_j$ for all $\mathbf{X} \in \mathbb{R}^I$. The two matrices \mathbb{M}^L and \mathbb{M}^H are used to approximate the identity operator. We assume that

$$(4.1) \quad 0 < m_i \quad \forall i \in \mathcal{V}, \quad m_i = \sum_{j \in \mathcal{V}(i)} m_{ji} \quad \forall i \in \mathcal{V},$$

to guarantee that \mathbb{M}^L and \mathbb{M}^H carry the same mass. This implies that $\sum_{i \in \mathcal{V}} m_i \mathbf{u}_i^n = \sum_{i \in \mathcal{V}} \sum_{j \in \mathcal{V}(i)} m_{ij} \mathbf{u}_j^n$ for all $\mathbf{u} \in (\mathbb{R}^{d+3})^I$, and $\sum_{i \in \mathcal{V}} m_i \mathbf{u}_i^n = \sum_{i \in \mathcal{V}} \sum_{j \in \mathcal{V}(i)} m_{ij} \mathbf{u}_j^n$ for all $\mathbf{u} \in (\mathbb{R}^{d+3})^I$. For instance, assuming that the approximation is done with continuous finite elements with global shape functions $\{\varphi_i\}_{i \in \mathcal{V}}$, then $m_i := \int_D \varphi_i(\mathbf{x}) \, dx$ and $m_{ij} := \int_D \varphi_i(\mathbf{x}) \varphi_j(\mathbf{x}) \, dx$. Letting $\mathbf{z}_h = \sum_{i \in \mathcal{V}} \mathbf{z}_i \varphi_i$ be the approximation of some smooth function $z : D \rightarrow \mathbb{R}$, we observe that $\int_D \varphi_i(\mathbf{x}) z(\mathbf{x}) \, dx \approx \int_D \varphi_i(\mathbf{x}) \mathbf{z}_h(\mathbf{x}) \, dx = \sum_{j \in \mathcal{V}(i)} m_{ij} \mathbf{z}_j \approx \sum_{j \in \mathcal{V}(i)} m_i \mathbf{z}_i$.

(iv) The underlying spatial discretization provides a $I \times I$, \mathbb{R}^d -valued matrix \mathbb{C} with the following properties. The entries of \mathbb{C} are denoted $\mathbf{c}_{ij} \in \mathbb{R}^d$ and are assumed to be such that $\mathbf{c}_{ij} = 0$ if $j \notin \mathcal{V}(i)$. For all $i \in \mathcal{V}(i)$, the coefficients $\{\mathbf{c}_{ij}\}_{j \in \mathcal{V}(i)}$ approximate the gradient operator on average in some reasonable sense. We further assume that

$$(4.2) \quad \mathbf{c}_{ij} = -\mathbf{c}_{ji} \quad \forall (i, j) \in \mathcal{V}^\circ \times \mathcal{V} \cup \mathcal{V} \times \mathcal{V}^\circ, \quad \sum_{j \in \mathcal{V}(i)} \mathbf{c}_{ij} = 0.$$

For instance, assuming that the approximation is done with continuous finite elements with global shape functions $\{\varphi_i\}_{i \in \mathcal{V}}$, then the coefficients $\mathbf{c}_{ij} := \int_D \varphi_i \nabla \varphi_j \, dx$ satisfy

this property. Indeed, letting $z_h = \sum_{i \in \mathcal{V}} z_i \varphi_i$ be the approximation of some function $z : D \rightarrow \mathbb{R}$, we observe that $\int_D \varphi_i(\mathbf{x}) \nabla z(\mathbf{x}) dx \approx \int_D \varphi_i(\mathbf{x}) \nabla z_h(\mathbf{x}) dx = \sum_{j \in \mathcal{V}(i)} z_j \mathbf{c}_{ij}$, which is the desired property. We also observe that $\mathbf{c}_{ij} = -\mathbf{c}_{ji}$ if $\varphi_i \varphi_j|_{\partial D} = 0$. The partition of unity implies property implies $\sum_{j \in \mathcal{V}(i)} \mathbf{c}_{ij} = 0$.

(v) The underlying spatial discretization provides a matrix $\mathbb{K}(\rho, T)$ with the following properties: $\mathbb{K}(\rho, T)$ is a real-valued $I \times I$ matrix approximating in some sense the diffusion operator $E_r \mapsto -\nabla \cdot \left(\frac{c}{3\sigma_t(\rho, T)} \nabla E_r \right)$. This matrix may depend on some given mass, ρ , and temperature distribution, T , or approximation thereof. The entries of $\mathbb{K}(\rho, T)$ are denoted $\mathbf{k}_{ij}(\rho, T)$. We finally assume that

$$(4.3) \quad \mathbf{k}_{ij} = -\mathbf{k}_{ji} \quad \forall (i, j) \in \mathcal{V}^2, \quad \mathbf{k}_{ij} \leq 0 \quad \forall j \in \mathcal{V}^*(i), \forall i \in \mathcal{V}, \quad \sum_{j \in \mathcal{V}(i)} \mathbf{k}_{ij} = 0 \quad \forall i \in \mathcal{V}.$$

For instance, with continuous finite elements and global shape functions $\{\varphi_i\}_{i \in \mathcal{V}}$, we have $\mathbf{k}_{ij}(\rho, T) := \int_D \frac{c}{3\sigma_t(\rho, T)} \nabla \varphi_i \cdot \nabla \varphi_j dx$. \square

Examples of discretization techniques satisfying the above assumptions are described in [18].

DEFINITION 4.2 (Conservation). *We say that a scheme $\{(\varrho_i^n, \mathbf{m}_i^{n\top}, \mathbf{E}_m^n, \mathbf{E}_r^n)\}_{i \in \mathcal{V}} \mapsto \{(\varrho_i^{n+1}, \mathbf{m}_i^{n+1\top}, \mathbf{E}_m^{n+1}, \mathbf{E}_r^{n+1})\}_{i \in \mathcal{V}}$ is conservative if*

$$\sum_{i \in \mathcal{V}} m_i \varrho_i^n = \sum_{i \in \mathcal{V}} m_i \varrho_i^{n+1}, \quad \sum_{i \in \mathcal{V}} m_i \mathbf{m}_i^n = \sum_{i \in \mathcal{V}} m_i \mathbf{m}_i^{n+1}, \quad \sum_{i \in \mathcal{V}} m_i \mathbf{E}_{\text{toti}}^n = \sum_{i \in \mathcal{V}} m_i \mathbf{E}_{\text{toti}}^{n+1}.$$

5. First-order IDP scheme. As our high-order scheme (not presented in this paper) is based on the combination of an IDP low-order method using forward and backward Euler time stepping with a high-order IMEX method, we first explain in this section how to construct the IDP low-order method. The method is composed of three stages. The first two stages approximate (3.3) and (3.6) using the forward Euler method, whereas the third stage solves (3.8) using a linearized version of the backward Euler method.

5.1. Hyperbolic stage 1. Let us assume that the approximation at time t^n of the solution to (2.1), say $\mathbf{u}_h^n := \sum_{j \in \mathcal{V}} \mathbf{u}_j^n \varphi_i$, is such that $\mathbf{u}_i^n \in \mathcal{A}(b)$ for all $i \in \mathcal{V}$ where $\mathcal{A}(b)$ is defined in (2.8). Let τ be the time step at t^n , and let us set $t^{n+1} := t^n + \tau$.

Our first goal is to construct a low-order IDP update $\mathbf{u}_h^{n+1} := \sum_{j \in \mathcal{V}} \mathbf{u}_j^{n+1} \varphi_i$ of the solution to the first hyperbolic stage (3.3). We essentially proceed as in [17] using the technique from Clayton et al. [9] to be able to use tabulated equations of states.

We first define the following low-order flux for all $i \in \mathcal{V}$ and all $j \in \mathcal{V}(i)$:

$$(5.1) \quad \mathbf{F}_{ij}^{L,n,1} := -(\mathbf{g}(\mathbf{u}_j^n) + \mathbf{g}(\mathbf{u}_i^n)) \mathbf{c}_{ij} + d_{ij}^{L,n,1} (\mathbf{u}_j^n - \mathbf{u}_i^n),$$

where $\mathbf{c}_{ij} \in \mathbb{R}^d$ is defined in §4, the flux \mathbf{g} is defined in (3.3), and the low-order graph viscosity coefficient $d_{ij}^{L,n,1}$ is defined by

$$(5.2) \quad d_{ij}^{L,n,1} := \max \left(\widehat{\lambda}_{\max}(\mathbf{n}_{ij}, \pi^1(\mathbf{u}_i^n), \pi^1(\mathbf{u}_j^n)), \widehat{\lambda}_{\max}(\mathbf{n}_{ji}, \pi^1(\mathbf{u}_j^n), \pi^1(\mathbf{u}_i^n)) \right).$$

Here, $\widehat{\lambda}_{\max}(\mathbf{n}, \pi^1(\mathbf{u}_L), \pi^1(\mathbf{u}_R))$ is any upper bound on the maximum wave speed in the Riemann problem with the extended flux $\widehat{\mathbf{g}}(\cdot) \mathbf{n}$, with $\widehat{\mathbf{g}}(\cdot)$ defined in (A.11), and

$$(5.3) \quad \pi^1(\mathbf{u}) := (\varrho, \mathbf{m} \cdot \mathbf{n}, \mathbf{E}_m - \frac{1}{2} (\|\mathbf{v}\|_{\ell^2}^2 - (\mathbf{v} \cdot \mathbf{n})^2), \mathbf{E}_r)^{\top}.$$

A source code providing a guaranteed upper bound $\widehat{\lambda}_{\max}(\mathbf{n}, \mathbf{u}_L, \mathbf{u}_R)$ for every pressure oracle satisfying (2.5) is available at [8]. We then define the low-order hyperbolic update $\mathbf{u}^{n,1}$ by setting

$$(5.4) \quad m_i \mathbf{u}_i^{n,1} = m_i \mathbf{u}_i^n + \tau \mathbf{F}_i^{\text{L},n,1}, \quad \mathbf{F}_i^{\text{L},n,1} := \sum_{j \in \mathcal{V}(i)} \mathbf{F}_{ij}^{\text{L},n,1}.$$

LEMMA 5.1 ($\mathbf{u}^n \mapsto \mathbf{u}^{n,1}$ is IDP & conservative). *Assume that the space discretization meets the structural assumptions (i)–(v) from Assumption 4.1. Assume that \mathbf{u}_i^n is in $\mathcal{A}(b)$ for all $i \in \mathcal{V}$. Assume that the time step satisfies $\tau \leq \max_{i \in \mathcal{V}} \cdot$. Let $\mathbf{u}^{n,1}$ be defined in (5.4). Then*

- (i) $\mathbf{u}_i^{n,1}$ is in $\mathcal{A}(b)$ for all $i \in \mathcal{V}$.
- (ii) The mapping $\mathbf{u}^n \mapsto \mathbf{u}^{n,1}$ is conservative.

Proof. See the proof of Theorem 4.6 in [9]. The conservation in the sense of Definition 4.2 is a consequence of the identity $\mathbf{c}_{ij} = -\mathbf{c}_{ij}$ which we assume to hold when either i or j is not a boundary degree of freedom; see Assumption 4.1(iv). \square

5.2. Hyperbolic stage 2. We continue with the approximation of the second hyperbolic stage (3.6). For every state $\mathbf{u} := (\varrho, \mathbf{m}^\top, \mathbf{E}_m, \mathbf{E}_r)^\top$, we define the reduced state $\mathbf{w} := (\varrho, \mathbf{m}^\top, \mathbf{E}_t)^\top$ where $\mathbf{E}_t := \mathbf{E}_r + \frac{1}{2} \varrho \|\mathbf{v}\|_{\ell^2}^2$ with $\mathbf{v} := \frac{\mathbf{m}}{\varrho}$.

Given the initial data $(\varrho^n, (\mathbf{m}^n)^\top, \mathbf{E}_m^n, \mathbf{E}_r^n)^\top$, we set $\mathbf{w}^n := (\varrho^n, (\mathbf{m}^n)^\top, \mathbf{E}_t^n)^\top$, with $\mathbf{E}_t^n := \mathbf{E}_r^n + \frac{1}{2} \varrho^n \|\mathbf{v}^n\|_{\ell^2}^2$. Next we define the low-order flux corresponding to the non-trivial part of the system of balance equations (3.6),

$$(5.5) \quad \mathbf{K}_{ij}^{\text{L},n,2} := -(\mathbb{k}(\mathbf{w}_j^n) + \mathbb{k}(\mathbf{w}_i^n)) \mathbf{c}_{ij} + d_{ij}^{\text{L},n,2}(\mathbf{w}_j^n - \mathbf{w}_i^n),$$

$$(5.6) \quad \mathbb{k}(\mathbf{w}) := (\mathbf{0}, p_r(\mathbf{w}) \mathbb{I}, \mathbf{v} p_r(\mathbf{w}))^\top, \quad \text{with} \quad p_r(\mathbf{w}) := \frac{1}{3} (\mathbf{E}_t - \frac{1}{2} \varrho \|\mathbf{v}\|_{\ell^2}^2).$$

The low-order graph viscosity coefficient $d_{ij}^{\text{L},n,2}$ is defined for all $i \in \mathcal{V}$, $j \in \mathcal{V}^*(i)$, by

$$(5.7) \quad d_{ij}^{\text{L},n,2} := \max(\widehat{\mu}_{\max}(\mathbf{n}_{ij}, \pi_{\mathbf{n}_{ij}}^2(\mathbf{w}_i^n), \pi_{\mathbf{n}_{ij}}^2(\mathbf{w}_j^n)), \widehat{\mu}_{\max}(\mathbf{n}_{ji}, \pi_{\mathbf{n}_{ij}}^2(\mathbf{w}_j^n), \pi_{\mathbf{n}_{ij}}^2(\mathbf{w}_i^n))),$$

where $\widehat{\mu}_{\max}(\mathbf{n}, \pi_{\mathbf{n}}^2(\mathbf{w}_L), \pi_{\mathbf{n}}^2(\mathbf{w}_R))$ is any upper bound on the maximum wave speed in the Riemann problem (B.1) with $\pi_{\mathbf{n}}^2(\mathbf{w}) := (\varrho, \varrho \mathbf{v} \cdot \mathbf{n}, \mathbf{E}_t - \frac{1}{2} \varrho \|\mathbf{v}\|_{\ell^2}^2 + \frac{1}{2} \varrho (\mathbf{v} \cdot \mathbf{n})^2)^\top$. Using the definition of \mathbf{E}_t , this also gives

$$(5.8) \quad \pi_{\mathbf{n}}^2(\mathbf{w}) = (\varrho, \varrho \mathbf{v} \cdot \mathbf{n}, \mathbf{E}_r + \frac{1}{2} \varrho (\mathbf{v} \cdot \mathbf{n})^2)^\top.$$

All the details regarding the computation of $\widehat{\mu}_{\max}$ are given in §B. We define the low-order hyperbolic update $\mathbf{w}^{n,2} := (\varrho^{n,2}, (\mathbf{m}^{n,2})^\top, \mathbf{E}_t^{n,2})^\top$ by setting

$$(5.9) \quad m_i \mathbf{w}_i^{n,2} := m_i \mathbf{w}_i^n + \tau \mathbf{K}_i^{\text{L},n,2}, \quad \mathbf{K}_i^{\text{L},n,2} := \sum_{j \in \mathcal{V}(i)} \mathbf{K}_{ij}^{\text{L},n,2}.$$

The update $\mathbf{u}^{n,2} := (\varrho^{n,2}, \mathbf{m}^{n,2}, \mathbf{E}_m^{n,2}, \mathbf{E}_r^{n,2})^\top$ is then obtained by setting

$$(5.10a) \quad \varrho^{n,2} := \varrho^{n,2},$$

$$(5.10b) \quad \mathbf{m}^{n,2} := \mathbf{m}^{n,2},$$

$$(5.10c) \quad \mathbf{E}_m^{n,2} := \mathbf{E}_m^n - \frac{1}{2} \varrho^n \|\mathbf{v}^n\|_{\ell^2}^2 + \frac{1}{2} \varrho^{n,2} \|\mathbf{v}^{n,2}\|_{\ell^2}^2,$$

$$(5.10d) \quad \mathbf{E}_r^{n,2} := \mathbf{E}_r^n - \frac{1}{2} \varrho^{n,2} \|\mathbf{v}^{n,2}\|_{\ell^2}^2.$$

The definitions of the updates (5.10c)-(5.10d) follow from (3.7). That is to say, the update (5.10d) is a materialization of the definition $E_t := E_r + \frac{1}{2}\varrho\|\mathbf{v}\|_{\ell^2}^2$, and the update (5.10c) defines $E_m^{n,2}$ by enforcing the internal energy, $E_m - \frac{1}{2}\varrho\|\mathbf{v}\|_{\ell^2}^2$, to be constant.

Remark 5.2 (Density update). Notice that although the conservation equation for the density is $\partial_t \rho = 0$, the update $\varrho^{n,2}$ is not equal to ϱ^n . The actual density update is given by $\varrho_i^{n,2} = \varrho_i^n + \frac{\tau}{m_i} \sum_{j \in \mathcal{V}(i)} d_{ij}^{L,n,2} (\varrho_j^n - \varrho_i^n)$. \square

LEMMA 5.3 ($\mathbf{u}^n \mapsto \mathbf{u}^{n,2}$ is IDP & conservative). *Assume that the structural assumptions (i)–(v) from Assumption 4.1 are met. Assume that \mathbf{u}_i^n is in $\mathcal{A}(b)$ for all $i \in \mathcal{V}$. Assume that the time step is chosen so that $\tau \leq \max_{i \in \mathcal{V}} \frac{2}{m_i} \sum_{j \in \mathcal{V}^*(i)} d_{ij}^{L,n,2}$. Let $\mathbf{u}^{n,2}$ be defined in (5.10) with $\mathbf{w}^{n,2}$ defined in (5.9). Then*

- (i) $\mathbf{u}_i^{n,2}$ is in $\mathcal{A}(b)$ for all $i \in \mathcal{V}$.
- (ii) The mapping $\mathbf{u}^n \mapsto \mathbf{u}^{n,2}$ is conservative.

Proof. We apply the generic theory developed in [17]; in particular, we invoke Theorem 4.1 therein. We start by defining

$$\bar{\mathbf{w}}_{ij}^n := \frac{1}{2}(\mathbf{w}_i^n + \mathbf{w}_j^n) - \frac{1}{2}(\mathbb{k}(\mathbf{w}_j^n) - \mathbb{k}(\mathbf{w}_i^n)) \cdot \mathbf{n}_{ij} \frac{\|\mathbf{c}_{ij}\|_{\ell^2}}{d_{ij}^{L,n,2}}.$$

After rearranging the terms in (5.9) and using that $\sum_{j \in \mathcal{V}(i)} \mathbf{c}_{ij} = 0$, we obtain

$$\mathbf{w}_i^{n,2} = \mathbf{w}_i^n \left(1 - \frac{2\tau}{m_i} \sum_{j \in \mathcal{V}^*(i)} d_{ij}^{L,n,2} \right) + \sum_{j \in \mathcal{V}^*(i)} \frac{2}{m_i} d_{ij}^{L,n,2} \bar{\mathbf{w}}_{ij}^n.$$

Thanks to the assumption we made on the time step, the above identity is a convex combination. Thanks to the definition of $\hat{\mu}_{\max}(\mathbf{n}_{ij}, \pi_{ij}^2(\mathbf{u}_i^n), \pi_{ij}^2(\mathbf{u}_j^n))$ and $d_{ij}^{L,n,2}$ it can be shown that $\bar{\mathbf{w}}_{ij}^n$ is a space average of the exact solution to the Riemann problem with flux $\mathbb{k}(\mathbf{v})\mathbf{n}_{ij}$ and with left state \mathbf{w}_i^n and right state \mathbf{w}_j^n . Let us consider the domain

$$\mathcal{R} := \{ \mathbf{w} := (\rho, \mathbf{m}^\top, E_t) \in \mathbb{R}^{d+2} \mid \rho > 0, 1 - b\rho > 0, E_t - \frac{1}{2}\rho\|\mathbf{v}\|_{\ell^2}^2 > 0 \}.$$

Since $\mathbf{u}_i^n \in \mathcal{A}(b)$ and $\mathbf{u}_j^n \in \mathcal{A}(b)$, we conclude that $\mathbf{w}_i^n \in \mathcal{R}$ and $\mathbf{w}_j^n \in \mathcal{R}$. As the domain \mathcal{R} is invariant under the action of the (entropy) solution operator of the Riemann problem and is convex, we conclude using Jensen's inequality that space averages of the exact solution to the Riemann problem remain in \mathcal{R} . This in turn implies that $\bar{\mathbf{w}}_{ij}^n$ is in \mathcal{R} . Invoking again the convexity of \mathcal{R} , we conclude that $\mathbf{w}_i^{n,2}$ is in \mathcal{R} because $\mathbf{w}_i^{n,2}$ is a convex combination of states in \mathcal{R} ; hence, the radiation energy of the state $\mathbf{u}_i^{n,2}$ defined in (5.10d) is positive. The internal energy of the state $\mathbf{u}_i^{n,2}$ defined in (5.10c) is above the cold curve because $\varrho_i^{n,2} e(\mathbf{u}_i^{n,2}) := E_m^{n,2} - \frac{1}{2}\varrho^{n,2}\|\mathbf{v}^{n,2}\|_{\ell^2}^2 := E_m^n - \frac{1}{2}\varrho^n\|\mathbf{v}^n\|_{\ell^2}^2 =: \varrho_i^n e(\mathbf{u}_i^n) > e_{\text{cold}}(\varrho_i^n)$. Likewise we have $0 < \varrho_i^{n,2}$, $0 < 1 - b\varrho_i^{n,2}$. In conclusion $\mathbf{u}_i^{n,2}$ is in $\mathcal{A}(b)$ for all $i \in \mathcal{V}$.

The conservation of mass and momentum in the sense of Definition 4.2 is a consequence of the identity $\mathbf{c}_{ij} = -\mathbf{c}_{ji}$ which we assume to hold when either i or j is not a boundary degree of freedom; see Assumption 4.1(iv). Let us now verify that the total energy is conserved. Adding (5.10c) and (5.10d) we obtain

$$E_{ri}^{n,2} + E_{mi}^{n,2} = E_{ti}^{n,2} + E_{mi}^n - \frac{1}{2}\varrho_i^n\|\mathbf{v}_i^n\|_{\ell^2}^2.$$

Summing over $i \in \mathcal{V}$ gives

$$\sum_{i \in \mathcal{V}} m_i E_{\text{toti}}^{n,2} = \sum_{i \in \mathcal{V}} m_i E_{ti}^{n,2} + \sum_{i \in \mathcal{V}} m_i (E_{mi}^n - \frac{1}{2}\varrho_i^n\|\mathbf{v}_i^n\|_{\ell^2}^2).$$

But $\sum_{i \in \mathcal{V}} m_i E_{ti}^{n,2} = \sum_{i \in \mathcal{V}} m_i E_{ti}^n$ because we assumed that $c_{ij} = -c_{ij}$ when either i or j is not a boundary degree of freedom; see Assumption 4.1(iv). The definition of E_{ti}^n gives $\sum_{i \in \mathcal{V}} m_i E_{ti}^n = \sum_{i \in \mathcal{V}} m_i (E_{ri}^n + \frac{1}{2} \varrho_i^n \|\mathbf{v}_i^n\|_{\ell^2}^2)$. Hence

$$\sum_{i \in \mathcal{V}} m_i E_{\text{toti}}^{n,2} = \sum_{i \in \mathcal{V}} m_i (E_{ri}^{n,2} + E_{mi}^n) = \sum_{i \in \mathcal{V}} m_i E_{\text{toti}}^n.$$

Hence, the total energy is conserved. This proves that the scheme is conservative. This completes the proof. \square

We now give some details on how to implement the second hyperbolic stage using the dependent variables $(\varrho, \mathbf{m}^\top, E_m, E_r)^\top$ instead of using $(\varrho, \mathbf{m}^\top, E_t)$, (5.9) and (5.10). Recalling that $E_t := E_r + \frac{1}{2} \varrho \|\mathbf{v}\|_{\ell^2}^2$, we define $\mathbf{F}_{ij}^{L,n,2} := (\mathbf{F}_{\varrho ij}^{L,2}, (\mathbf{F}_{\mathbf{m} ij}^{L,2})^\top, \mathbf{F}_{E_m ij}^{L,2}, \mathbf{F}_{E_r ij}^{L,2})^\top$ and $\mathbf{B}_i^{L,n,2} := (\mathbf{B}_{\varrho i}^{L,2}, (\mathbf{B}_{\mathbf{m} i}^{L,2})^\top, \mathbf{B}_{E_m i}^{L,2}, \mathbf{B}_{E_r i}^{L,2})^\top$ where

$$(5.11a) \quad \begin{cases} \mathbf{F}_{\varrho ij}^{L,n,2} = d_{ij}^{L,n,2} (\varrho_j^n - \varrho_i^n), \\ \mathbf{F}_{\mathbf{m} ij}^{L,n,2} = -\mathbf{c}_{ij} (p_r(E_{r,j}^n) + p_r(E_{r,i}^n)) + d_{ij}^{L,n,2} (\mathbf{m}_j^n - \mathbf{m}_i^n), \\ \mathbf{F}_{E_m ij}^{L,n,2} = 0, \\ \mathbf{F}_{E_r ij}^{L,n,2} = -\mathbf{c}_{ij} \cdot (\mathbf{v}_j^n p_r(E_{r,j}^n) + \mathbf{v}_i^n p_r(E_{r,i}^n)) + d_{ij}^{L,n,2} (E_{t,j}^n - E_{t,i}^n) \end{cases}$$

$$(5.11b) \quad \begin{cases} \mathbf{B}_{\varrho i}^{L,n,2} = 0, \\ \mathbf{B}_{\mathbf{m} i}^{L,n,2} = 0, \\ \mathbf{B}_{E_m i}^{L,n,2} = m_i \frac{\varrho_i^{n,2}}{2} (\|\mathbf{v}_i^{n,2}\|_{\ell^2}^2 - \|\mathbf{v}_i^n\|_{\ell^2}^2), \\ \mathbf{B}_{E_r i}^{L,n,2} = -m_i \frac{\varrho_i^{n,2}}{2} (\|\mathbf{v}_i^{n,2}\|_{\ell^2}^2 - \|\mathbf{v}_i^n\|_{\ell^2}^2). \end{cases}$$

Then the update (5.10) can be rewritten into the following equivalent form:

$$(5.12) \quad m_i \mathbf{u}_i^{n,2} = m_i \mathbf{u}_i^n + \tau \mathbf{F}_i^{L,n,2} + \mathbf{B}_i^{L,n,2}, \quad \mathbf{F}_i^{L,n,2} := \sum_{j \in \mathcal{V}(i)} \mathbf{F}_{ij}^{L,n,2}.$$

Notice that in (5.12) the velocity $\mathbf{v}_i^{n,2}$ has to be updated before updating $E_{m,i}^{n,2}$ and $E_{r,i}^{n,2}$ because the sources $\mathbf{B}_{E_m i}^{L,n,2}$ and $\mathbf{B}_{E_r i}^{L,n,2}$ depend on $\mathbf{v}_i^{n,2}$; see (5.11b).

5.3. Multiplicative vs. additive splitting. The hyperbolic update, $\mathbf{u}^{h,n}$, can be realized in two different ways: either multiplicative or additive. We now discuss these two options. It turns out that the additive update is the most robust method.

5.3.1. Multiplicative splitting. The multiplicative version of the hyperbolic update, $\mathbf{u}^{h,n}$, consists of handling the hyperbolic stages 1 and 2 in a sequential way, where stage 1 is followed by stage 2 (or vice versa). This multiplicative process can be symbolically represented by $\mathbf{u}^n \mapsto \mathbf{u}^{n,1} \mapsto \mathbf{u}^{n,2} =: \mathbf{u}^{h,n}$ where the time step τ for this explicit algorithm depends on the state \mathbf{u}^n . The technical difficulty with this process is that the time step τ for steps 1 and 2 must be identical and the second hyperbolic step can be guaranteed to be IDP only if $\tau \leq \max_{i \in \mathcal{V}} \frac{2}{m_i} \sum_{j \in \mathcal{V}^*(i)} d_{ij}^{L,n,2}$ where $d_{ij}^{L,n,2}$ is defined in (5.7); hence, the time step τ a priori depends on the result of stage 1. This means that the time step is implicitly defined. Hence, the multiplicative splitting does not have a guaranteed way to choose τ so the mapping $\mathbf{u}^n \mapsto \mathbf{u}^{n,1} \mapsto \mathbf{u}^{n,2} =: \mathbf{u}^{h,n}$ is invariant-domain preserving.

5.3.2. Additive splitting. A better way to proceed, often advocated in the literature, is to make the splitting additive. Given the state \mathbf{u}^n , we define $\mathbf{w}^n := (\varrho^n, (\mathbf{m}^n)^\top, \mathbf{E}_t^n)^\top$, with $\mathbf{E}_t^n := \mathbf{E}_r^n + \frac{1}{2}\varrho^n \|\mathbf{v}^n\|_{\ell^2}^2$. Then for all $i \in \mathcal{V}$ and all $j \in \mathcal{V}^*(i)$, we define

$$(5.13a) \quad d_{ij}^{\text{L},n,1} := \max \left(\widehat{\lambda}_{\max}(\mathbf{n}_{ij}, \pi_{ij}^1(\mathbf{u}_i^n), \pi_{ij}^1(\mathbf{u}_j^n)), \widehat{\lambda}_{\max}(\mathbf{n}_{ji}, \pi_{ij}^1(\mathbf{u}_j^n), \pi_{ij}^1(\mathbf{u}_i^n)) \right).$$

$$(5.13b) \quad d_{ij}^{\text{L},n,2} := \max \left(\widehat{\mu}_{\max}(\mathbf{n}_{ij}, \pi_{ij}^2(\mathbf{w}_i^n), \pi_{ij}^2(\mathbf{w}_j^n)), \widehat{\mu}_{\max}(\mathbf{n}_{ji}, \pi_{ij}^2(\mathbf{w}_j^n), \pi_{ij}^2(\mathbf{w}_i^n)) \right),$$

and introduce the two time steps

$$(5.14) \quad \tau_1 := \max_{i \in \mathcal{V}} \frac{2}{m_i} \sum_{j \in \mathcal{V}^*(i)} d_{ij}^{\text{L},n,1}, \quad \tau_2 := \max_{i \in \mathcal{V}} \frac{2}{m_i} \sum_{j \in \mathcal{V}^*(i)} d_{ij}^{\text{L},n,2}.$$

Notice that depending on the Mach number, the two time steps τ_1 and τ_2 may be significantly different. We then define

$$(5.15) \quad \theta := \frac{\tau_2}{\tau_1 + \tau_2}, \quad \tau := \frac{\tau_1 \tau_2}{\tau_1 + \tau_2}.$$

Notice that these definitions imply that $\tau = \theta \tau_1$, $\tau = (1 - \theta) \tau_2$, and $\tau < \min(\tau_1, \tau_2)$. Using the notation described in (5.4) and (5.9), we define the additive updates

$$(5.16a) \quad \mathbf{u}^{n,1} = \mathbf{u}^n + \frac{\tau}{m_i \theta} \mathbf{F}^{\text{L},n,1},$$

$$(5.16b) \quad \mathbf{u}^{n,2} = \mathbf{u}^n + \frac{\tau}{m_i (1 - \theta)} \mathbf{F}^{\text{L},n,2} + \mathbf{B}_i^{\text{L},n,2},$$

where $\mathbf{F}^{\text{L},n,1}$, $\mathbf{F}^{\text{L},n,2}$, and $\mathbf{B}_i^{\text{L},n,2}$ are constructed using the same state initial \mathbf{u}^n . Notice that $\mathbf{u}^{n,1}$ is the first hyperbolic update realized with the time step τ_1 , and $\mathbf{u}^{n,2}$ is the second hyperbolic update realized with the time step τ_2 . The final hyperbolic update $\mathbf{u}^{\text{h},n}$ is defined by

$$(5.17) \quad \mathbf{u}^{\text{h},n} := \theta \mathbf{u}^{n,1} + (1 - \theta) \mathbf{u}^{n,2}.$$

THEOREM 5.4 ($\mathbf{u}^n \mapsto \mathbf{u}^{\text{h},n}$ is IDP & conservative). *Assume that the space discretization meets the structural assumptions (i)–(v) from Assumption 4.1. Assume that \mathbf{u}_i^n is in $\mathcal{A}(b)$ for all $i \in \mathcal{V}$. Assume that the time step is chosen so that $\tau \leq \frac{\tau_1 \tau_2}{\tau_1 + \tau_2}$ with τ_1 and τ_2 defined in (5.13). Let $\mathbf{u}^{\text{h},n}$ be defined in (5.17). Then*

- (i) $\mathbf{u}_i^{\text{h},n}$ is in $\mathcal{A}(b)$ for all $i \in \mathcal{V}$.
- (ii) The mapping $\mathbf{u}^n \mapsto \mathbf{u}^{\text{h},n}$ is conservative.

Proof. Notice that $\mathbf{u}^n \mapsto \mathbf{u}^{n,1}$ is conservative and the mapping is IDP because $\frac{\tau}{\theta} = \tau \frac{\tau_1 + \tau_2}{\tau_2} = \tau_1$. The same argument holds for $\mathbf{u}^n \mapsto \mathbf{u}^{n,2}$ because $\frac{\tau}{1 - \theta} = \tau \frac{\tau_1 + \tau_2}{\tau_1} = \tau_2$. Observe finally that $\mathbf{u}^{\text{h},n}$ is a convex combination of two states that are IDP and conservative. \square

All the tests reported in the paper are done with the additive update.

5.4. Parabolic stage. We finally focus our attention on the solution to the parabolic stage (3.8). Given the state $\mathbf{u}^{\text{h},n} := (\varrho^{\text{h},n}, \mathbf{m}^{\text{h},n}, \mathbf{E}_m^{\text{h},n}, \mathbf{E}_r^{\text{h},n})^\top$, we define the specific internal energy $\mathbf{e}^{\text{h},n} := \frac{1}{\varrho^{\text{h},n}} (\mathbf{E}_m^{\text{h},n} - \frac{1}{2} \varrho^{\text{h},n} \|\mathbf{v}^{\text{h},n}\|_{\ell^2}^2)$. Recalling the relation between the temperature and the internal energy (2.6) given by the oracle, we set $\mathbf{T}^{\text{h},n} := T(\varrho^{\text{h},n}, \mathbf{e}^{\text{h},n})$. To account for the dependency of the other coefficients with

respect to the temperature, we use a standard linearization process; see e.g., Knoll et al. [23, Eqs. (18)-(19)], Knoll et al. [24, Eqs. (42)-(43)]. We denote by \mathbf{T}^* a positive and yet to be computed estimation of \mathbf{T}^{n+1} , and we set $\sigma_a^{h,n}(\mathbf{T}^*) := \sigma_a(\varrho^{h,n}, \mathbf{T}^*)$, $c_v^{h,n}(\mathbf{T}^*) := c_v(\varrho^{h,n}, \mathbf{T}^*)$ where the average heat capacity at constant volume c_v is defined in (2.7). The coefficients of the matrix $\mathbb{K}(\varrho^{h,n}, \mathbf{T}^*)$ introduced in Assumption 4.1(v) are denoted $k_{ik}^{h,n}(\mathbf{T}^*)$.

Let $\mathbf{u}^{n+1} := (\varrho^{n+1}, \mathbf{m}^{n+1}, \mathbf{E}_m^{n+1}, \mathbf{E}_r^{n+1})^\top$ be the low-order parabolic update. Given $\mathbf{T}^* > 0$ (yet to be clearly defined), we update $(\mathbf{T}^{n+1})_{i \in \mathcal{V}}$ and $(\mathbf{E}_r^{n+1})_{i \in \mathcal{V}}$ by solving the following discrete counterpart of (3.8):

$$(5.18a) \quad \varrho_i^{h,n} (c_v^{h,n}(\mathbf{T}_i^*) \mathbf{T}_i^{n+1} - c_v^{h,n}(\mathbf{T}_i^{h,n}) \mathbf{T}_i^{h,n}) = -\tau \sigma_a^{h,n}(\mathbf{T}^*) c (a_r[\mathbf{T}_i^*]^3 \mathbf{T}_i^{n+1} - \mathbf{E}_{r,i}^{n+1}),$$

$$(5.18b) \quad m_i (\mathbf{E}_{r,i}^{n+1} - \mathbf{E}_{r,i}^{h,n}) + \tau (\mathbb{K}(\varrho^{h,n}, \mathbf{T}^*) \mathbf{E}^{n+1})_i = \tau m_i \sigma_a^{h,n}(\mathbf{T}_i^*) c (a_r[\mathbf{T}_i^*]^3 \mathbf{T}_i^{n+1} - \mathbf{E}_{r,i}^{n+1}).$$

Finally, recalling (2.7) we set $\mathbf{e}^{n+1} := c_v(\varrho^{h,n}, \mathbf{T}^*) \mathbf{T}^{n+1} + \mathbf{e}_{\text{cold}}(\varrho^{h,n})$. The mechanical energy and the other components of the parabolic update are obtained by setting

$$(5.19) \quad \varrho^{n+1} := \varrho^{h,n}, \quad \mathbf{m}^{n+1} := \mathbf{m}^{h,n}, \quad \mathbf{E}_m^{n+1} := \varrho^{n+1} (\mathbf{e}^{n+1} + \frac{1}{2} \|\mathbf{v}^{n+1}\|_{\ell^2}^2),$$

$$(5.20) \quad \text{with } \mathbf{e}^{n+1} := c_v(\varrho^{n+1}, \mathbf{T}^*) \mathbf{T}^{n+1} + \mathbf{e}_{\text{cold}}(\varrho^{h,n}).$$

LEMMA 5.5 ($\mathbf{u}^{h,n} \mapsto \mathbf{u}^{n+1}$ is IDP & conservative). *Assume that the space discretization meets the structural assumptions (i)-(v) from Assumption 4.1. Assume that $\mathbf{T}_i^* > 0$ for all $i \in \mathcal{V}$. Then*

- (i) *The system (5.18) is linear and has a unique solution.*
- (ii) *The low-order parabolic update $\mathbf{u}^{h,n} \mapsto \mathbf{u}^{n+1}$ is IDP for all $\tau > 0$.*
- (iii) *The scheme $\mathbf{u}^{h,n} \mapsto \mathbf{u}^{n+1}$ is conservative.*

Proof. Re-arranging the terms in (5.18a) yields

$$(5.21) \quad \mathbf{T}_i^{n+1} = \frac{\varrho_i^{h,n} c_v^{h,n}(\mathbf{T}_i^{h,n}) \mathbf{T}_i^{h,n} + \tau \sigma_a^{h,n}(\mathbf{T}_i^*) c \mathbf{E}_{r,i}^{n+1}}{\varrho_i^{h,n} c_v^{h,n}(\mathbf{T}_i^*) + \tau \sigma_a^{h,n}(\mathbf{T}_i^*) c a_r[\mathbf{T}_i^*]^3},$$

which proves that the dependency $\mathbf{E}_r^{n+1} \mapsto \mathbf{T}^{n+1}$ is affine. Hence, the system (5.18) is linear. The identity (5.21) proves that the new temperature \mathbf{T}_i^{n+1} is positive once we establish that $\mathbf{E}_r^{n+1} \geq 0$, which we now prove. Substituting (5.21) into (5.18b) gives

$$(5.22) \quad m_i \left(1 + \frac{\tau \sigma_a^{h,n}(\mathbf{T}_i^*) c \varrho_i^{h,n} c_v^{h,n}(\mathbf{T}_i^*)}{\varrho_i^{h,n} c_v^{h,n}(\mathbf{T}_i^{h,n}) + \tau \sigma_a^{h,n}(\mathbf{T}_i^*) c a_r[\mathbf{T}_i^*]^3} \right) \mathbf{E}_{r,i}^{n+1} + \tau \sum_{j \in \mathcal{V}(i)} k_{ij}^{h,n}(\mathbf{T}^*) \mathbf{E}_{r,j}^{n+1} = \\ m_i \underbrace{\left(\mathbf{E}_{r,i}^{h,n} + \frac{\tau \sigma_a^{h,n}(\mathbf{T}_i^*) c \varrho_i^{h,n} c_v^{h,n}(\mathbf{T}_i^{h,n})}{\varrho_i^{h,n} c_v^{h,n}(\mathbf{T}_i^{h,n}) + \tau \sigma_a^{h,n}(\mathbf{T}_i^*) c a_r[\mathbf{T}_i^*]^3} a_r[\mathbf{T}_i^*]^3 \mathbf{T}_i^{h,n} \right)}_{>0}.$$

Let \mathbb{G} be the $I \times I$ matrix with entries $\mathbb{G}_{ij} := m_i (1 + \frac{\tau m_i \sigma_a^{h,n}(\mathbf{T}_i^*) c \varrho_i^{h,n} c_v^{h,n}(\mathbf{T}_i^*)}{\varrho_i^{h,n} c_v^{h,n}(\mathbf{T}_i^{h,n}) + \tau \sigma_a^{h,n}(\mathbf{T}_i^*) c a_r[\mathbf{T}_i^*]^3}) \delta_{ij} + \tau k_{ij}^{h,n}$. Since $k_{ij}^{h,n} \leq 0$ for all $j \in \mathcal{V}^*(i)$, we conclude that \mathbb{G} is a Z -matrix; see (4.3). Since $\sum_{j \in \mathcal{V}(i)} k_{ij}^{h,n} = 0$, we conclude that \mathbb{G} is an M -matrix; see e.g., [14, Lem. 28.17]. Hence, \mathbb{G} is invertible and the system (5.18) has a unique solution.

Since the inverse of \mathbb{G} has nonnegative entries and the right-hand side in (5.22) is positive, we infer that $\mathbf{E}_{r,i}^{n+1} > 0$ for all $i \in \mathcal{V}$. More precisely, we have

$$\min_{i \in \mathcal{V}} \mathbf{E}_{r,i}^{n+1} \geq \min_{i \in \mathcal{V}} \frac{\mathbf{E}_{r,i}^{h,n} + \frac{\tau \sigma_a^{h,n}(\mathbf{T}_i^*) c \varrho_i^{h,n} c_v^{h,n}(\mathbf{T}_i^{h,n})}{\varrho_i^{h,n} c_v^{h,n}(\mathbf{T}_i^{h,n}) + \tau \sigma_a^{h,n}(\mathbf{T}_i^*) c a_r[\mathbf{T}_i^*]^3} a_r[\mathbf{T}_i^*]^3 \mathbf{T}_i^{h,n}}{1 + \frac{\tau \sigma_a^{h,n}(\mathbf{T}_i^*) c \varrho_i^{h,n} c_v^{h,n}(\mathbf{T}_i^{h,n})}{\varrho_i^{h,n} c_v^{h,n}(\mathbf{T}_i^{h,n}) + \tau \sigma_a^{h,n}(\mathbf{T}_i^*) c a_r[\mathbf{T}_i^*]^3}} \geq \min_{i \in \mathcal{V}} (\mathbf{E}_{r,i}^{h,n}, a_r[\mathbf{T}_i^*]^3 \mathbf{T}_i^{h,n}).$$

Then (5.21) implies that $T_i^{n+1} > 0$ for all $i \in \mathcal{V}$. Using the relation (5.20), i.e., $e_i^{n+1} = c_v^{h,n}(\varrho_i^{n+1}, T_i^{n+1}) + e_{\text{cold}}(\varrho_i^{n+1})$, we infer that the internal energy is above the cold curve. In conclusion, the new state \mathbf{u}_i^{n+1} is in $\mathcal{A}(b)$ for all $i \in \mathcal{V}$. This proves that the low-order parabolic stage $\mathbf{u}^{h,n} \mapsto \mathbf{u}^{n+1}$ is IDP.

Summing (5.18a) and (5.18b), summing over $i \in \mathcal{V}$, and using $k_{ij}^{h,n}(T^*) = k_{ji}^{h,n}(T^*)$ together with $\sum_{j \in \mathcal{V}(i)} k_{ij}^{h,n}(T^*) = 0$ from (4.3), we obtain

$$\sum_{i \in \mathcal{V}} m_i (e_i^{n+1} + E_r^{n+1}) = \sum_{i \in \mathcal{V}} m_i (e_i^{h,n} + E_r^{h,n}).$$

Since the density and the momentum are unchanged in the parabolic stage, i.e., $\frac{1}{2} \varrho_i^{n+1} \|\mathbf{v}_i^{n+1}\|_{\ell^2}^2 = \frac{1}{2} \varrho_i^{h,n} \|\mathbf{v}_i^{h,n}\|_{\ell^2}^2$, this implies that the total energy is conserved. This completes the proof. \square

Now the key question that we have to address is how T_i^* should be estimated. At low the Mach numbers, it is well known that just using $T_i^* = T^n$ or $T_i^* = T^{h,n}$ is sufficient in the sense that this simple choice does not restrict too much the time step. But this is no longer the case at large Mach numbers. Hence, similarly to [23, 24] we propose to use an iterative process to estimate T^* that is robust with respect to the Mach number. But contrary to what is usually done in the literature, we do not solve the coupled problem (5.18) using a Newton-Krylov method. We instead have observed that using a fixed-point Picard iteration method is sufficient to solve (5.18), even at very high Mach numbers. The algorithm that we propose proceeds as follows: (i) initialize the process with $T_i^* = T_i^n$; (Do not use $T_i^* = T_i^{h,n}$. Robustness is lost by using $T_i^* = T_i^{h,n}$ since at steady state $T_i^{n+1} = T_i^n \neq T_i^{h,n}$.); (ii) Compute the update E^{n+1} by solving (5.22); (iii) Then update T_i^* for all $i \in \mathcal{V}$ by solving the nonlinear equation

$$(5.23) \quad m_i \varrho_i^{h,n} c_v^{h,n}(T_i^*) (T_i^* - T_i^{h,n}) = -\tau m_i \sigma_a^{h,n}(T^*)_i c (a_r [T_i^*]^4 - E_{r,i}^{n+1}).$$

This can be done with Newton's algorithm using the current value of T_i^* as initial guess; (iv) Repeat steps (ii)-(iii) until some tolerance is achieved. Finally, update T_i^{n+1} for all $i \in \mathcal{V}$ using (5.21) to ensure conservation of the total energy. A detailed version of the algorithm is shown in Algorithm 5.1.

Algorithm 5.1 Parabolic update (T^{n+1}, E^{n+1})

Require: $\mathbf{u}^{h,n}$, T^n

Initialize: $T^* = T^n$; $\sigma_{a,\text{ref}}$; $E_{r,\text{ref}}$; ϵ ;
 $\text{err} := 10^{30}$; $\epsilon^N := \epsilon \times \tau \times \sigma_{a,\text{ref}} \times c \times E_{r,\text{ref}}$

while $\text{err} > \epsilon$ **do**

 Update E_r^{n+1} by solving (5.22)
 $T^{*,\text{old}} = T^*$

for $i \in \mathcal{V}$ **do**

 Let T_i^* solve (5.23) up to residual tolerance ϵ^N (Newton algorithm)
 $\text{err} = \|T^* - T^{*,\text{old}}\|_{\ell^1} / \|T^{*,\text{old}}\|_{\ell^1}$

 Update T^{n+1} using (5.21) with $T^{*,\text{old}}$.

 Update ϱ^{n+1} , \mathbf{m}^{n+1} and E_m using (5.19)

5.5. Conclusion. Combining Theorem 5.4 with Lemma 5.5 we have proved the following result.

THEOREM 5.6. *Assume that the space discretization meets the structural assumptions (i)–(v) from Assumption 4.1. Assume that \mathbf{u}_i^n is in $\mathcal{A}(b)$ for all $i \in \mathcal{V}$. Assume that the time step is chosen so that $\tau \leq \frac{\tau_1 \tau_2}{\tau_1 + \tau_2}$ with τ_1 and τ_2 defined in (5.13). Let $\mathbf{u}^{h,n}$ be defined in (5.17). Let $\epsilon > 0$ and \mathbf{u}^{n+1} be defined by Algorithm 5.1 using (5.1)–(5.22)–(5.23). Then the two stage algorithm $\mathbf{u}^n \mapsto \mathbf{u}^{h,n} \mapsto \mathbf{u}^{n+1}$ has the following properties for all $\epsilon > 0$:*

- (i) *It is IDP.*
- (ii) *It is conservative.*

Proof. Owing to the time step restriction $\tau \leq \frac{\tau_1 \tau_2}{\tau_1 + \tau_2}$ and Theorem 5.4, the mapping $\mathbf{u}^n \mapsto \mathbf{u}^{h,n}$ is IDP (in addition to being conservative). Moreover, we have established in Lemma 5.5 that $\mathbf{u}^{h,n} \mapsto \mathbf{u}^{n+1}$ is IDP. Let now prove that the mapping $\mathbf{u}^{h,n} \mapsto \mathbf{u}^{n+1}$ is also conservative. As the mass and momentum are unchanged in the parabolic step, we just have to prove that $\sum_{i \in \mathcal{V}} m_i \mathbf{E}_{\text{tot},i}^{n+1} = \sum_{i \in \mathcal{V}} m_i \mathbf{E}_{\text{tot},i}^{h,n}$ if there is no energy influx at the boundary. Let $\mathbf{T}_i^{*,\text{old}}$ be the penultimate temperature defined in Algorithm 5.1. Adding $m_i \times (5.18\text{a})$ and (5.18b), using that $\varrho^{n+1} := \varrho^{h,n}$, $\mathbf{v}_i^{n+1} := \mathbf{v}_i^{h,n}$, and using the definition of $\mathbf{E}_{\text{m},i}^{n+1}$ in (5.19), we obtain

$$\begin{aligned} -\tau (\mathbb{K}(\rho^{h,n}, \mathbf{T}^{*,\text{old}}) \mathbf{E}^{n+1})_i &= m_i (\mathbf{E}_{\text{r},i}^{n+1} + \varrho_i^{h,n} c_v^{h,n} (\mathbf{T}_i^{*,\text{old}}) \mathbf{T}_i^{n+1} \\ &\quad - \mathbf{E}_{\text{r},i}^{h,n} - \varrho_i^{h,n} c_v^{h,n} (\mathbf{T}_i^{h,n}) \mathbf{T}_i^{h,n}) \\ &= m_i \left(\mathbf{E}_{\text{r},i}^{n+1} + \varrho_i^{n+1} c_v(\varrho_i^{n+1}, \mathbf{T}_i^{*,\text{old}}) \mathbf{T}_i^{n+1} + e_{\text{cold}}(\varrho_i^{n+1}) + \frac{1}{2} \|\mathbf{v}_i^{n+1}\|_{\ell}^2 \right. \\ &\quad \left. - (\mathbf{E}_{\text{r},i}^{h,n} + \varrho_i^{h,n} c_v(\varrho_i^{h,n}, \mathbf{T}_i^{h,n}) \mathbf{T}_i^{h,n} + e_{\text{cold}}(\varrho_i^{h,n}) + \frac{1}{2} \|\mathbf{v}_i^{h,n}\|_{\ell}^2) \right) \\ &= m_i (\mathbf{E}_{\text{r},i}^{n+1} + \mathbf{E}_{\text{m},i}^{n+1} - \mathbf{E}_{\text{tot},i}^{h,n} - \mathbf{E}_{\text{m},i}^{h,n}) = m_i (\mathbf{E}_{\text{tot},i}^{n+1} - \mathbf{E}_{\text{tot},i}^{h,n}) \end{aligned}$$

Hence, if $\sum_{i \in \mathcal{V}} m_i (\mathbb{K}(\rho^{h,n}, \mathbf{T}^{*,\text{old}}) \mathbf{E}^{n+1})_i = 0$, i.e., there is no energy influx at the boundary, the total energy is conserved $\sum_{i \in \mathcal{V}} m_i \mathbf{E}_{\text{tot},i}^{n+1} = \sum_{i \in \mathcal{V}} m_i \mathbf{E}_{\text{tot},i}^{h,n}$ thereby proving that $\sum_{i \in \mathcal{V}} m_i \mathbf{E}_{\text{tot},i}^{n+1} = \sum_{i \in \mathcal{V}} m_i \mathbf{E}_{\text{tot},i}^n$. \square

6. Numerical results. We now verify that the first-order, conservative IDP approximation of the model (2.1) presented in the paper performs as advertised.

6.1. Preliminaries. The numerical tests are performed with two separate codes to verify reproducibility. The first code, henceforth called `code1`, is written in Fortran 95/2003 and does not use any particular software. It uses meshes composed of simplices (triangles in 2D and tetraedron in 3D). The second is a high-performance code, `ryujin` (henceforth referred to as `code2`), see [19, 30], built upon the `deal.II` finite element library [1]. It is written in C++ and uses cuboids (quadrangles in 2D and hexahedrons in 3D). Both codes reproduce the algorithm described in the paper using the additive splitting described in (5.13)–(5.17) for the explicit hyperbolic stage followed by the implicit parabolic stage described in Algorithm 5.1. The space approximation in `code1` is done with continuous \mathbb{P}_1 finite elements. The space approximation in `code2` is done with continuous \mathbb{Q}_1 finite elements. The time step τ is systematically computed in both codes with (5.15) using the definition

$$(6.1) \quad \tau := \text{CFL} \frac{\tau_1 \tau_2}{\tau_1 + \tau_2}.$$

where $\text{CFL} \in (0, 1]$ is the user-dependent Courant–Friedrichs–Lewy number. Unless specified otherwise the relative tolerance in Algorithm 5.1 is set to $\epsilon = 10^{-5}$.

In all the tests for which an analytical solutions exists, we compute the error at time t as follows:

$$(6.2) \quad \text{err}(t) := \frac{\|\rho_h(\cdot, t) - \rho(\cdot, t)\|_{L^1(D)}}{\|\rho(\cdot, T)\|_{L^1(D)}} + \frac{\|\mathbf{m}_h(\cdot, t) - \mathbf{m}(\cdot, t)\|_{L^1(D)}}{\|\mathbf{m}(\cdot, T)\|_{L^1(D)}} \\ + \frac{\|E_{mh}(\cdot, t) - E_m(\cdot, t)\|_{L^1(D)}}{\|E_m(\cdot, t)\|_{L^1(D)}} + \frac{\|E_{rh}(\cdot, t) - E_r(\cdot, t)\|_{L^1(D)}}{\|E_r(\cdot, t)\|_{L^1(D)}},$$

where ρ_h , \mathbf{m}_h , E_{mh} , and E_{rh} are the approximate density, momentum, mechanical energy, and radiation energy, and ρ , \mathbf{m} , E_m , and E_r are the exact density, momentum, mechanical energy, and radiation energy.

6.2. Units. Although the system (2.1) can be made non-dimensional by proceeding as in Bolding et al. [4], we are going to follow the literature and report results using dimensional quantities. Unless stated otherwise, we use the following units. Length scales and distances are measured in cm. Scattering and absorption cross sections are measured in cm^{-1} . Masses are measured in g. Time is measured in shake sh (called shakes for plural). One shake sh is equal to 1×10^{-8} s. Energies are measured in GJ. Recall that one giga-Joule is equal to 1×10^9 J. Pressures are measured in GJ/cm^3 ; recall that one GJ/cm^3 is equal to 10 Gbar.

The temperatures are rescaled by the Boltzmann constant k , i.e., we use $\tilde{T} := kT$ instead of T , and the temperatures thus rescaled are measured in kiloelectronvolt keV. Recall that one eV is also an energy unit and $1 \text{ eV} := 1.602 176 634 \times 10^{-19} \text{ J}$; hence, the ratio $1 \text{ J}/1 \text{ eV}$ is dimensionless.

The radiation constant $a_r := \frac{4\sigma}{c}$ is also rescaled, instead of using a_r we use $\tilde{a}_r := a_r/k^4$. The rescaled radiation constant is measured in $\text{GJ}/\text{cm}^3 \text{ keV}^4$.

The specific heat capacities at constant volume is also rescaled by the Boltzmann constant, i.e., we use $\tilde{c}_v := c_v/k$ instead of c_v , and the rescaled specific heat capacity is measured in $\text{GJ}/(\text{g keV})$ where GJ is the giga-Joule unit. We recall that for ideal gases the heat capacity is given by $c_v = \frac{1}{\gamma-1} k \text{Na} \frac{Z_{\text{eff}}+1}{A}$, where γ is the heat capacity ratio, Na is the Avogadro number, Z_{eff} is effective nuclear charge (also called effective ionization state) and A is the atomic mass. We use the ideal gas equation of state in all the tests reported in the paper, and we arbitrarily choose $\frac{Z_{\text{eff}}+1}{A}$ so that $\tilde{c}_v = 1.5 \times 10^{-1} \text{ GJ}/\text{keV g}$, and unless stated otherwise, we use $\gamma = \frac{5}{3}$.

The constants used in the following numerical tests are reported in Table 6.1. The speed of light and the rescaled radiation constant reported therein are copied

Table 6.1: Units

speed of light c	$2.997 924 58 \times 10^2 \text{ cm/sh}$
rescaled radiation constant \tilde{a}_r	$1.372 017 2 \times 10^{-2} \text{ GJ}/(\text{cm}^3 \text{ keV}^4)$
heat capacity ratio γ	$\frac{5}{3}$ or $\gamma = 1.2$ for Mach 50 test
rescaled heat capacity \tilde{c}_v	$1.5 \times 10^{-1} \text{ GJ}/\text{keV g}$

verbatim from the **ExactPack** software [25], Thrussell and Ferguson [37].

6.3. Marshak wave. We start by considering a simplified version of the problem (2.1) to verify the correctness of the approximation of the parabolic stage. As in Pomraning [34, Eq. (1)&(5)], we neglect the fluid motion and solve the system

$$(6.3a) \quad \partial_t(\rho c_v T) = -\sigma_a c(a_r T(\mathbf{u})^4 - E_r),$$

$$(6.3b) \quad \partial_t E_r + -\nabla \cdot (\frac{c}{3\sigma_a} \nabla E_r) = \sigma_a c(a_r T(\mathbf{u})^4 - E_r),$$

where the density ρ is constant. We use the same setting as in Larsen et al. [26, §7]. The computational domain is $D := (0, \ell_D)$ with $\ell_D = 2.5 \times 10^{-2}$ cm. We take $\rho = 2 \text{ g/cm}^3$, and the constant \tilde{c}_v , \tilde{a}_r and c are given in Table 6.1. We use $\sigma_t = \sigma_a = 300(\frac{T_{\text{ref}}}{T})^3$ with $T_{\text{ref}} = 1 \text{ keV}$. The initial data are $T_0 = 1 \times 10^{-2} \text{ keV}$ and $E_{r,0} = \tilde{a}_r T_0^4$. We enforce the Dirichlet boundary $E_r(0, t) = \tilde{a}_r T_{\text{ref}}^4$ and the homogeneous Neumann boundary condition $\partial_x E_r(\ell_D, t) = 0$ for all $t > 0$. The approximation is done by using the algorithm described in the paper without invoking the hyperbolic update (i.e., at the beginning of §5.4 we set $\mathbf{u}^{h,n} := (\varrho, \mathbf{0}, \mathbf{E}_m^n, \mathbf{E}_r^n)^T$).

The composite relative error in the L^1 -norm (defined in (6.2)) is computed with an approximation of the exact solution at the final time $t = 2 \times 10^{-2}$ sh using `code1` on a uniform mesh composed of 20 001 grid points. We show in Table (6.2) the composite relative L^1 -error for 6 uniform meshes. We use $\text{CFL} = 0.25$ in all the simulation (the algorithm is L^2 -stable irrespective of the value of CFL). We observe first order convergence in the asymptotic regime for both `code1` and `code2`. We plot the solution

code1			code2		
I	L^1 -error	rate	I	L^1 -error	rate
65	2.95×10^{-3}	—	65	3.94×10^{-3}	—
129	2.27×10^{-3}	0.38	129	4.27×10^{-3}	-0.11
257	1.52×10^{-3}	0.58	257	2.62×10^{-3}	0.71
513	9.11×10^{-4}	0.74	513	1.57×10^{-3}	0.73
1025	5.00×10^{-4}	0.87	1025	6.36×10^{-4}	1.31
2049	2.83×10^{-4}	0.82	2049	3.47×10^{-4}	0.88

Table 6.2: Marshak wave problem (6.3). Exact solution approximated with `code1` and 20 001 grid points. Composite relative L^1 -error at $t = 2 \times 10^{-2}$ sh for 6 meshes with $\text{CFL} = 0.25$.

profiles using `code2` for the Marshak wave for the temperature (left) and radiation energy (right).

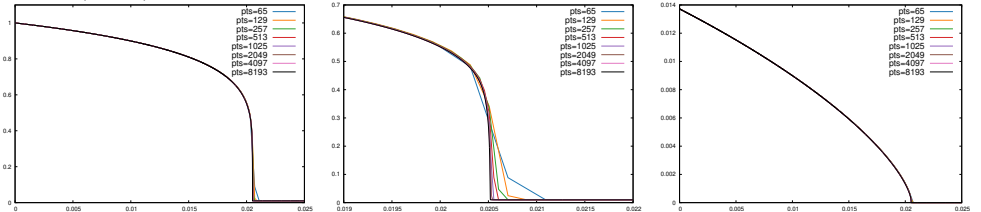


Figure 6.1: Marshak wave with $\sigma_t = 300(\frac{T_{\text{ref}}}{T})^3$ at $T = 0.02$ sh. Left: temperature. Center: zoom in on temperature shock location. Right: radiation energy.

6.4. 1D radiative shocks. We now consider common steady radiative shock configurations found in the literature (see Delchini et al. [12], Lowrie and Edwards [28]). All the tests reported in this section are performed with `code1`. We have verified that `code2` gives the same results (not reported for brevity). For all the configurations the reference density is $\rho_{\text{ref}} = 1 \text{ g cm}^{-3}$ and the reference temperature is $T_{\text{ref}} = 0.1 \text{ keV}$. Given γ , ρ_{ref} , T_{ref} and a prescribed Mach number, the semi-analytic steady radiative shock solution is computed with the methodology described in [28]

using the **ExactPack** software [25, 37] developed at Los Alamos National Laboratory. To shorten the time to reach steady state we initialize every simulation by interpolating the semi-analytic solution obtained from **ExactPack** using 10^6 uniform grid points. Unless stated otherwise, we run all the tests with the Courant–Friedrichs–Lowy number CFL = 1.

6.4.1. Subcritical tests. We first consider the Mach 1.2 and Mach 3 radiative shock cases which are categorized as “subcritical” in [28]. The computational domain is $D = (-0.02, 0.02 \text{ cm})$. Dirichlet boundary conditions are enforced. The tests are performed on a sequence of uniform meshes. We assume that $\sigma_t = 500 \text{ cm}^{-1}$ and $\sigma_a = 500 \text{ cm}^{-1}$, i.e., $\sigma_s = 0$. The final time is set to $t = 1 \text{ sh}$. This time is long enough for steady state to be reached.

$\sigma_a = \sigma_t = 500 \text{ cm}^{-1}$			$\sigma_a = \sigma_t = 500 \frac{\rho T_{\text{ref}}^{3.5}}{\rho_{\text{ref}} T^{3.5}} \text{ cm}^{-1}$		
I	Mach 1.2	Mach 3	I	Mach 3	–
101	8.14×10^{-2}	8.31×10^{-2}	101	7.83×10^{-2}	–
201	4.16×10^{-2}	0.97	201	3.91×10^{-2}	1.01
401	2.05×10^{-2}	1.02	401	1.89×10^{-2}	1.05
801	1.01×10^{-2}	1.02	801	9.14×10^{-3}	1.05
1601	5.01×10^{-3}	1.01	1601	4.54×10^{-3}	1.01
3201	2.50×10^{-3}	1.00	3201	2.25×10^{-3}	1.01
6401	1.25×10^{-3}	1.00	6401	1.10×10^{-3}	1.03
12801	6.31×10^{-4}	0.99	12801	5.30×10^{-4}	1.05

Table 6.3: Left table: L^1 errors and convergence rates for 1D radiative shock with $\sigma_a = 500 \text{ cm}^{-1}$ and $\sigma_s = 0$ for Mach 1.2 and 3 respectively. Right table: L^1 errors and convergence rates for 1D radiative shock with $\sigma_a = 500 \frac{\rho}{\rho_{\text{ref}}} \left(\frac{T_{\text{ref}}}{T} \right)^{3.5} \text{ cm}^{-1}$ and $\sigma_s = 0$ for Mach 3.

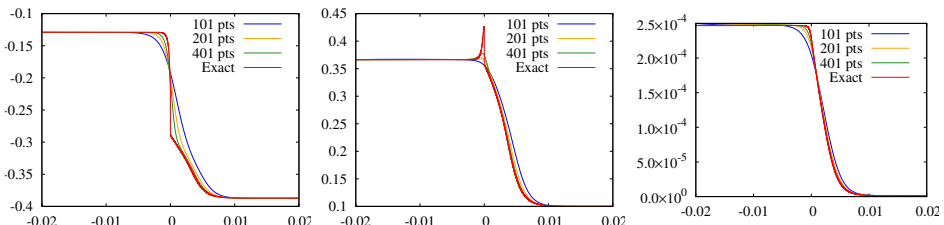


Figure 6.2: Mach 3 radiative shock with $\sigma_t = 500 \text{ cm}^{-1}$ at $T = 1 \text{ sh}$. Left: velocity. Center: temperature. Right: radiation energy.

In Table 6.3, we report the cumulative L^1 -norm error defined in (6.2) for Mach numbers 1.2 and 3, respectively. We observe first-order rate as expected. In Figure 6.2, we plot the numerical velocity, material temperature and radiation energy for the Mach 3 configuration using 101, 201, and 401 grid points and we compare the results to the semi-analytic solution.

We also report in Table 6.3 a test done at Mach 3 with the opacity depending on ρ and T ; see e.g., Delchini et al. [13, §4.4] or Lowrie and Edwards [28, Fig. 17]. More specifically; we take $\sigma_t = \sigma_a = 500 \frac{\rho}{\rho_{\text{ref}}} \left(\frac{T}{T_{\text{ref}}} \right)^{-3.5} \text{ cm}^{-1}$. In this case the computational

domain is $D = (-0.3, 0.3 \text{ cm})$. The simulations are run up to $t = 10 \text{ sh}$ to reach steady state. The nonlinear dependency of the cross section with respect to the density and the temperature makes the zone out of thermodynamics equilibrium larger (see temperature peak in the center panel of Figure 6.3 and compare to Figure 6.2). The convergence rates are reported in the right table in Table 6.3. We observe first order convergence in this case as well.

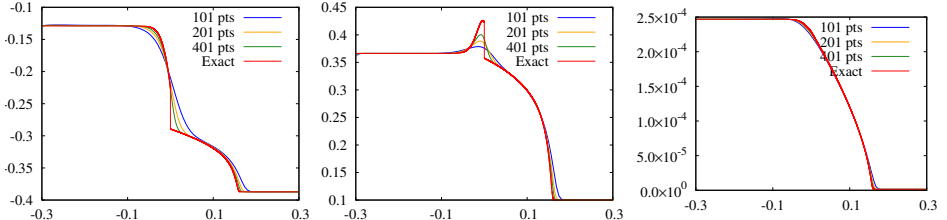


Figure 6.3: Mach 3 radiative shock with $\sigma_a = 500 \frac{\rho}{\rho_{\text{ref}}} \left(\frac{T_{\text{ref}}}{T} \right)^{3.5} \text{ cm}^{-1}$ and $\sigma_s = 0$ for Mach 3. Left: velocity. Center: temperature. Right: radiation energy.

6.4.2. Supercritical tests. Now, we consider the Mach 10, Mach 30, and Mach 50 radiative shock cases which are categorized as “supercritical” in [28].

$\sigma_a = \sigma_t = 500 \text{ cm}^{-1}$						$\sigma_a = \sigma_t = 500 \frac{T_{\text{ref}} \rho}{\rho_{\text{ref}} T} \text{ cm}^{-1}$					
I	Mach 30			Mach 50			I	Mach 10			
101	1.58×10^{-1}	–	–	1.75×10^{-1}	–	–	101	1.15×10^{-1}	–	–	
201	9.03×10^{-2}	0.81	9.51×10^{-2}	0.88	–	–	201	5.76×10^{-2}	1.01	–	
401	4.79×10^{-2}	0.92	5.47×10^{-2}	0.80	–	–	401	3.05×10^{-2}	0.92	–	
801	2.61×10^{-2}	0.88	3.03×10^{-2}	0.85	–	–	801	1.62×10^{-2}	0.92	–	
1601	1.39×10^{-2}	0.91	1.67×10^{-2}	0.87	–	–	1601	7.72×10^{-3}	1.07	–	
3201	7.30×10^{-3}	0.93	9.35×10^{-3}	0.83	–	–	3201	3.96×10^{-3}	0.96	–	
6401	3.79×10^{-3}	0.94	5.03×10^{-3}	0.89	–	–	6401	9.96×10^{-4}	1.00	–	
12801	1.98×10^{-3}	0.94	2.66×10^{-3}	0.92	–	–	12801	1.98×10^{-3}	0.92	–	

Table 6.4: Left table: L^1 errors and convergence rates for 1D radiative shock with $\sigma_a = \sigma_t = 500 \text{ cm}^{-1}$ and $\sigma_s = 0$ for Mach 30 and 50, respectively. Right table: L^1 errors and convergence rates for 1D radiative shock with $\sigma_a = \sigma_t = 500 \frac{T_{\text{ref}} \rho}{\rho_{\text{ref}} T} \text{ cm}^{-1}$ and $\sigma_s = 0$ for Mach 10.

The computational domain for the Mach 10 case is $D = (-2, 5 \text{ cm})$ and we use density and temperature dependent opacities $\sigma_t = \sigma_a = 500 \frac{\rho}{\rho_{\text{ref}}} \left(\frac{T}{T_{\text{ref}}} \right)^{-3.5} \text{ cm}^{-1}$. The simulation time to reach steady state is $t = 50 \text{ sh}$. The computational domain for Mach 30 is $D = (-0.1, 0.4 \text{ cm})$ and we use $\sigma_t = \sigma_a = 500 \text{ cm}^{-1}$. The simulation time to reach steady state in this case is $t = 1 \text{ sh}$. The domain for Mach 50 is $D = (-0.1, 0.6 \text{ cm})$ and we use $\sigma_t = \sigma_a = 500 \text{ cm}^{-1}$. The simulation time to reach steady state in this case is $t = 10 \text{ sh}$. We use $\gamma = 1.2$ for the Mach 50 case only (the solution process used in the **ExactPack** software is ill-posed for $\gamma = \frac{5}{3}$ at Mach 50). These tests are again performed on a sequence of uniform meshes. The final time is set to $T = 1 \text{ sh}$. In the left panel of Table 6.4, we report the cumulative L^1 -norm

error for the tests at Mach numbers 30 and 50. We show in the right panel of the table the cumulative L^1 -norm error for the tests at Mach numbers 10. In all the case we observe the first-order rate as expected.

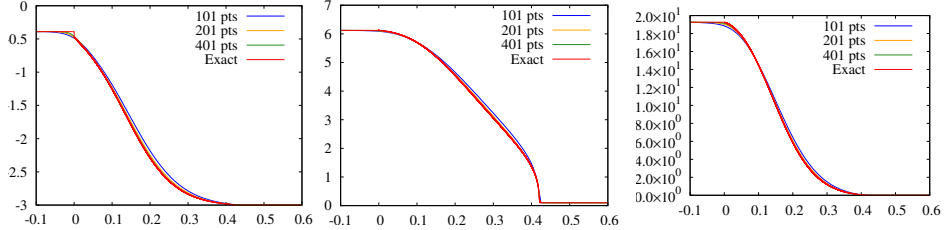


Figure 6.4: Mach 50 radiative shock with $\sigma_a = \sigma_t = 500 \text{ cm}^{-1}$ at $t = 10 \text{ sh}$. Left: velocity. Center: temperature. Right: radiation energy.

In Figure 6.4, we plot the numerical velocity, material temperature and radiation energy for the Mach 50 configuration.

6.5. ICF-like configuration. We finish by simulating a setting loosely inspired from an indirect drive inertial confinement fusion experiment in one and two dimensions in a hohlraum device, see e.g., Olson et al. [33]. Our objective is not to be close to one particular experiment but instead to give some feeling on how the method behaves when solving a problem with data that are in a realistic range.

6.6. Setting. We model the transverse cross section of the hohlraum by a disk $D = \{\mathbf{x} \in \mathbb{R}^d \mid \|\mathbf{x}\|_{\ell^2} < r_{\text{ext}}\}$ centered at $\mathbf{0}$ of radius $r_{\text{ext}} := 0.3 \text{ cm}$. A spherical pellet with a high-density carbon shell contains a light material (either gas or solid deuterium). The outside of the pellet is composed of a low pressure gas. In the indirect drive setting considered here, radiation energy is injected into the domain through the boundary of D using Dirichlet boundary conditions. The slip boundary condition on the velocity is enforced at the boundary of D . We simplify the setting by modeling all the materials with the same ideal gas equation of state with $\gamma = \frac{5}{3}$. We now summarize the geometry, initial conditions, and boundary conditions:

$$(6.4) \quad \begin{aligned} r_{\text{int}} &:= 1.3 \times 10^{-1} \text{ cm}, & r_{\text{sh}} &:= 1.5 \times 10^{-1} \text{ cm}, & r_{\text{ext}} &:= 6 \times 10^{-1} \text{ cm}, \\ \rho_{\text{int}} &:= 5 \times 10^{-4} \text{ g/cm}^3, & \rho_{\text{sh}} &:= 3.5 \text{ g/cm}^3, & \rho_{\text{ext}} &:= 1 \times 10^{-4} \text{ g/cm}^3, \\ T_{\text{int}} &:= 2.6 \times 10^{-6} \text{ keV}, & T_{\text{ref}} &:= 2.5 \times 10^{-1} \text{ keV}, & \gamma &= \frac{5}{3}, \\ \rho_{\text{ref}} &:= 1 \text{ g/cm}^3, & \sigma_{\text{ref}} &:= 5 \times 10^3 \text{ cm}^{-1}, & \sigma_a(\rho) &= \sigma_t(\rho) = \frac{\rho}{\rho_{\text{ref}}} \sigma_{\text{ref}}. \end{aligned}$$

$$(6.5) \quad \rho_0(\mathbf{x}), \mathbf{u}_0(\mathbf{x}), T_0(\mathbf{x}), E_{\text{r},0}(\mathbf{x}) = \begin{cases} \rho_{\text{int}}, \mathbf{0}, T_{\text{int}}, a_{\text{r}} T_{\text{int}}^4 & \|\mathbf{x}\|_{\ell^2} < r_{\text{int}} \\ \rho_{\text{sh}}, \mathbf{0}, \frac{\rho_{\text{int}}}{\rho_{\text{sh}}} T_{\text{int}}, a_{\text{r}} (\frac{\rho_{\text{int}}}{\rho_{\text{sh}}}) T_{\text{int}}^4 & \|\mathbf{x}\|_{\ell^2} < r_{\text{sh}} \\ \rho_{\text{ext}}, \mathbf{0}, \frac{\rho_{\text{int}}}{\rho_{\text{ext}}} T_{\text{int}}, a_{\text{r}} T_{\text{ref}}^4 & \text{otherwise.} \end{cases}$$

$$(6.6) \quad \mathbf{u} \cdot \mathbf{n}|_{\partial D} = 0, \quad E_{\text{r}}|_{\partial D} = a_{\text{r}} T_{\text{ref}}^4.$$

6.7. One-dimensional case. We start by solving the problem in one space dimension. Although to account for the spherical nature of the pellet, the problem should be solved in spherical coordinates, we work with the Cartesian coordinate system as our objective is just to demonstrate the robustness of the method.

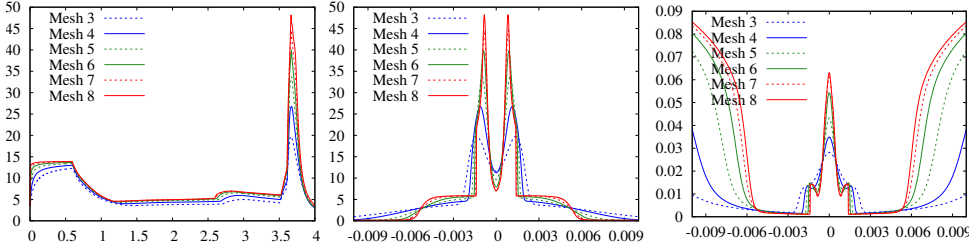


Figure 6.5: 1D ICF. Left: time history of maximum density. Center: density profile at the time maximum density is reached. Right: temperature at the time maximum density is reached. Mesh3 has 4097 grid points and Mesh8 has 131073 grid points.

The computational domain is $D = (-r_{\text{ext}}, r_{\text{ext}})$ with $r_{\text{ext}} := 0.6$ cm. The problem is solved on various uniform meshes with increasing number of grid points to verify that convergence occurs. The simulation time is $t = 4$ sh. We show in Figure 6.5 the time history of the maximum density for six meshes $(\text{mesh}_i)_{i \in \{3:8\}}$ with number of grid points equal to 2^{9+i} using `code1`. We observe in the left panel of the figure that the maximum density rises very quickly after initialization due to a very strong compression wave crossing the high-density carbon (this wave is clearly visible in the left panel in Figure 6.6). The time for this wave to cross the high-density carbon is approximately 0.6 sh. The left and right compression waves then travel in the interior material and make contact at approximately 2.15 sh. At this time the compression process starts and reaches its maximum at about 3.67 sh. By inspecting the left panel we observe that this time depends very little of the mesh resolution, but the actual value of the maximum density at this time can only be well captured on very fine grids. We show in the center and right panels of Figure 6.5 closeup views of the density and temperature fields in the interval $(-0.01, 0.01)$ cm at the time 3.67 sh when the density peak reaches its maximum. These results are well reproduced with `code2` and are therefore not reported for brevity.

6.8. Two-dimensional case. We finish with two-dimensional simulations of the ICF problem keeping the setting described in §6.6. Again, the problem should be solved in cylindrical coordinates, but we use Cartesian coordinates for simplicity.

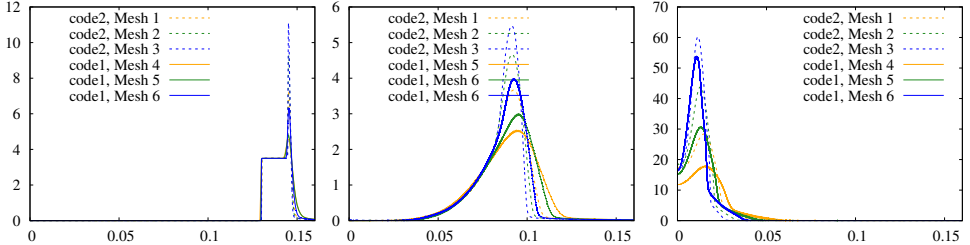


Figure 6.6: Density vs. r . Left to right: $t = 0.1$ sh; $t = 2$ sh; $t = 3.7$ sh.

The simulations using `code1` are done on three meshes composed of nonuniform triangular Delaunay meshes (Mesh4: 115,079 grid points, Mesh5: 330,735 grid points, Mesh6: 1,261,299 grid points). The results are compared to the simulations done with

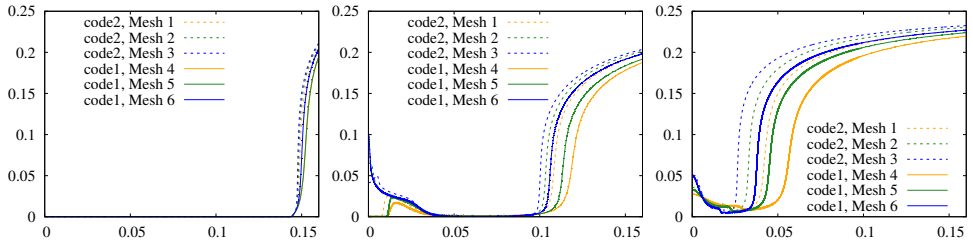


Figure 6.7: Temperature vs. r . Left to right: $t = 0.1$ sh; $t = 2$ sh; $t = 3.7$ sh

code2 using three quadrangular meshes (Mesh 1: 786,945, Mesh 2: 3,146,753, Mesh 3: 12,584,961). All the meshes (triangular and quadrangular) are more refined in the shell and the interior region than in the exterior region. We show in Figure 6.6 and Figure 6.7 the scatter plots of the density and temperature as functions of the radius $r := \|\mathbf{x}\|_{\ell^2}$ for the seven meshes in the range $r \in [0, 0.16]$ and for times 0.1 sh, 2 sh, and 3.7 sh. We observe that cylindrical symmetry is well preserved for all the fields.

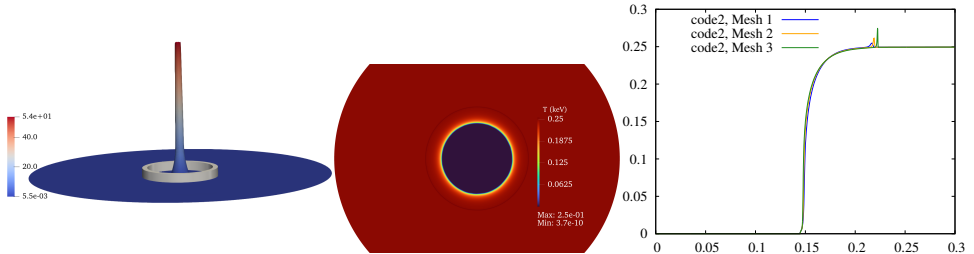


Figure 6.8: Left: 3D rendering of the density density field; the density at $t = 0$ is shown is solid color; the density at $t = 3.7$ sh is shown in color (code1, Mesh6). Right: temperature at $t = 0.1$; notice the faint circular black line which is a Zeldovich spike.

We further show in the left panel of Figure 6.8 a three-dimensional rendering of the density field at $t = 0.1$ sh (solid color) and $t = 3.7$ sh (using the cool to warm color palette). We show the temperature field at $t = 0.1$ sh in the center panel. We observe in the temperature profile the Zeldovich spike propagating outwards away from the center (black line in the red background). We highlight the Zeldovich spike in the right panel in Figure 6.8 by plotting again the temperature profile over the radius range $r \in [0, 0.3]$.

Appendix A. First hyperbolic problem and Riemann problem. We focus in this section on the hyperbolic problem (3.3). We recall here the technique that is introduced in Clayton et al. [9] to construct an invariant-domain preserving approximation of the problem for any equation of state satisfying the generic assumptions (2.5) with the domain $\mathcal{B}(b)$ defined in (2.4). The key is to construct auxiliary states with the desired properties.

A.1. Abstract Riemann problem and bar states. Since the technique we are going to present in this section is quite general, we change notation for a moment and assume that one wants to solve a general hyperbolic system with some generic flux $\mathbf{g} : \mathcal{G} \rightarrow \mathbb{R}^{s \times d}$, $s \geq 1$, where \mathcal{G} , the domain of \mathbf{g} , is a subset of \mathbb{R}^s . Given two

states $\mathbf{u}_L, \mathbf{u}_R$ in \mathcal{G} , a unit vector \mathbf{n} in \mathbb{R}^d , and a positive real number λ , we consider the following auxiliary states (also called bar states hereafter):

$$(A.1) \quad \bar{\mathbf{u}}_{LR}(\lambda) := \frac{1}{2}(\mathbf{u}_L + \mathbf{u}_R) - \frac{1}{2\lambda}(\mathbf{g}(\mathbf{u}_R)\mathbf{n} - \mathbf{g}(\mathbf{u}_L)\mathbf{n}).$$

To be able to extract information regarding $\bar{\mathbf{u}}_{LR}(\lambda)$, it is useful to consider the following Riemann problem:

$$(A.2) \quad \partial_t \mathbf{w} + \partial_x(\mathbf{g}(\mathbf{w})\mathbf{n}) = 0, \quad \mathbf{w}(x, 0) = \begin{cases} \mathbf{u}_L & \text{if } x < 0, \\ \mathbf{u}_R & \text{if } 0 \leq x. \end{cases}$$

Recall that (A.2) may have infinitely many weak solutions and weak solutions to (A.2) are self-similar. For every self-similar weak solution, \mathbf{v} , there exists a number $\lambda_{\max}^{\mathbf{v}} > 0$, called maximum wave speed, so that $\mathbf{v}(\frac{x}{t}) = \mathbf{u}_L$ if $x \leq -\lambda_{\max}^{\mathbf{v}}t$ and $\mathbf{v}(\frac{x}{t}) = \mathbf{u}_R$ if $\lambda_{\max}^{\mathbf{v}}t \leq x$. The following result, proved in Lemma 2.1 and Lemma 2.2 in [17] (see also Lemma 3.2 in Clayton et al. [9]) and largely inspired from the work of P. Lax, A. Harten, E. Tadmor et al. (see Remark A.3), explains the connection between (A.1) and (A.2).

LEMMA A.1. *Let $\mathbf{u}_L, \mathbf{u}_R$ be two arbitrary states in \mathcal{G} . Let $\mathbf{v}(\frac{x}{t})$ be any self-similar weak solution to (A.2). Let $\lambda_{\max}^{\mathbf{v}}$ be the maximum wave speed for this weak solution. Let us set $\bar{\mathbf{v}}(t) := \int_{-\frac{1}{2}}^{\frac{1}{2}} \mathbf{v}(\frac{x}{t}) dx$ for all $t > 0$. Let $\lambda > 0$ and assume that $\lambda \geq \lambda_{\max}^{\mathbf{v}}$. Then*

$$(A.3) \quad \bar{\mathbf{u}}_{LR}(\lambda) = \bar{\mathbf{v}}(\frac{1}{2\lambda}),$$

(A.4) *If \mathcal{G} is convex and $\mathbf{v}(\xi) \in \mathcal{G}$ for all $\xi \in \mathbb{R}$, then $\bar{\mathbf{u}}_{LR}(\lambda) \in \mathcal{G}$,*

(A.5) *Let (η, \mathbf{q}) be an entropy pair. If \mathbf{v} is s.t. $\partial_t \eta(\mathbf{v}) + \partial_x(\mathbf{q}(\mathbf{v})\mathbf{n}) \leq 0$, then*

$$\eta(\bar{\mathbf{u}}_{LR}(\lambda)) \leq \frac{1}{2}(\eta(\mathbf{u}_L) + \eta(\mathbf{u}_R)) - \frac{1}{2\lambda}(\mathbf{q}(\mathbf{u}_R)\mathbf{n} - \mathbf{q}(\mathbf{u}_L)\mathbf{n}).$$

Let $\mathbf{v}(\frac{x}{t})$ be any self-similar weak solution to (A.2), then (A.3) says that $\bar{\mathbf{u}}_{LR}(\lambda)$ is equal to the average of \mathbf{v} over the interval $(-\frac{1}{2}, \frac{1}{2})$ if $\lambda \geq \lambda_{\max}^{\mathbf{v}}$. As a result, the statement in (A.4) says that under the assumptions that \mathcal{G} is convex and the weak solution \mathbf{v} leaves \mathcal{G} invariant, then $\bar{\mathbf{u}}_{LR}(\lambda) \in \mathcal{G}$ as well. Finally, (A.5) says that if the weak solution \mathbf{v} satisfies an entropy inequality for some pair (η, \mathbf{q}) , then $\bar{\mathbf{u}}_{LR}(\lambda)$ satisfies a discrete counterpart of this inequality.

Unfortunately, the Riemann problem (A.2) cannot be solved analytically in general. But, a key observation made in [9] that allows us to go around this roadblock is that it is not necessary to solve (A.2) to extract useful information on the bar states (A.1). One can instead consider a surrogate Riemann problem that is solvable and somewhat interpolates \mathbf{g} as we now explain. We take inspiration from [9] and introduce an extension technique that will facilitate this interpolation process.

We assume that we have at hand a new integer $\hat{s} \geq s$, an extension operator $\Theta : \mathbb{R}^s \rightarrow \mathbb{R}^{\hat{s}}$, an extended flux $\hat{\mathbf{g}} : \hat{\mathcal{D}} \rightarrow \mathbb{R}^{\hat{s} \times d}$, and a linear reduction operator $\Pi : \mathbb{R}^{\hat{s}} \rightarrow \mathbb{R}^s$, so that the following identities hold true:

$$(A.6a) \quad \Pi(\Theta(\mathbf{w})) = \mathbf{w}, \quad \forall \mathbf{w} \in \mathcal{G},$$

$$(A.6b) \quad \Pi(\hat{\mathbf{g}}(\Theta(\mathbf{w}))\mathbf{n}) = \mathbf{g}(\mathbf{w})\mathbf{n}, \quad \forall \mathbf{w} \in \mathcal{G}, \quad \forall \mathbf{n}.$$

Notice that the triple $(\hat{s} = s, \Pi = I_d, \Theta = I_d)$, where I_d is the identity operator, trivially satisfies the above assumption, thereby showing that the class of objects we

are considering is not empty. Note that (A.6a) implies that Θ is a right inverse of Π . Finally we consider the following extended Riemann problem:

$$(A.7) \quad \partial_t \widehat{\mathbf{w}} + \partial_x (\widehat{\mathbf{g}}(\widehat{\mathbf{w}}) \mathbf{n}) = 0, \quad \widehat{\mathbf{w}}(x, 0) = \begin{cases} \Theta(\mathbf{u}_L) & \text{if } x < 0, \\ \Theta(\mathbf{u}_R) & \text{if } 0 \leq x. \end{cases}$$

For future reference we also introduce the bar state associated with (A.7):

$$(A.8) \quad \bar{\mathbf{u}}_{LR}(\lambda) := \frac{1}{2}(\Theta(\mathbf{u}_L) + \Theta(\mathbf{u}_R)) - \frac{1}{2\lambda}(\widehat{\mathbf{g}}(\Theta(\mathbf{u}_R)) \mathbf{n} - \widehat{\mathbf{g}}(\Theta(\mathbf{u}_L)) \mathbf{n}).$$

Of course the above somewhat obscure construction has the potential to be useful only if solving (A.7) is significantly easier than solving (A.2). We show below that it is indeed the case for the problem (3.3). The following result is essential and shows how the bar states $\bar{\mathbf{u}}_{LR}(\lambda)$ and $\bar{\mathbf{u}}_{LR}(\lambda)$ are related.

LEMMA A.2 (Extended bar state). *Assume that the assumptions (A.6) are met. Then the following identity holds true for all pairs $(\mathbf{u}_L, \mathbf{u}_R) \in \mathcal{G}^2$ and all $\lambda > 0$:*

$$(A.9) \quad \Pi(\bar{\mathbf{u}}_{LR}(\lambda)) = \bar{\mathbf{u}}_{LR}(\lambda).$$

Proof. Apply the operator Π on both sides of the definition (A.8), use the linearity of Π , and conclude using (A.6). \square

Hence, to establish that $\bar{\mathbf{u}}_{LR}(\lambda) \in \mathcal{G}$, it suffices to find a pair of operators (Π, Θ) and an extended flux $\widehat{\mathbf{g}}$ for which the extended Riemann problem (A.7) can be easily solved, and such that $\Pi(\bar{\mathbf{u}}_{LR}(\lambda)) \in \mathcal{G}$.

Remark A.3 (Literature). The states $\bar{\mathbf{u}}_{LR}(\lambda)$ are the backbone of Lax's scheme. The importance of these states has been recognized in Nessyahu and Tadmor [32, Eq. (2.6)]. It is established in Harten et al. [21, §3.A] that these states are averages of Riemann solutions provided $\lambda \geq \lambda_{\max}$. The idea of extending the Riemann problem to simplify the estimation of λ_{\max} (see (A.6)) has its origins in Clayton et al. [9, §3] where this construction is used to estimate a guaranteed upper bound on the maximum wave speed in the Riemann problem associated with the compressible Euler equation supplemented with an arbitrary equation of state. The above abstract construction with the operators Π , Θ and the extended flux $\widehat{\mathbf{g}}$ generalizes [9, §3]. \square

A.2. Extended flux and Riemann problem. We present in this section one possible extension of the Riemann problem (A.2) with \mathbf{g} defined in (3.3). This is done by proceeding as in [9, §3]. For simplicity we assume that the pressure oracle is such that the pressure is positive and the cold curve is zero. We refer to Clayton and Tovar [7] and [20] for generalizations removing these restrictions but still using the above theoretical setting.

We set $s := d + 3$ and $\widehat{s} := s + 1$. We define the operators Π and Θ as follows:

$$(A.10a) \quad \Pi : \mathbb{R}^{\widehat{s}} \ni \widehat{\mathbf{u}} := (\rho, \mathbf{m}^T, E_m, E_r, \Gamma)^T \mapsto \Pi(\widehat{\mathbf{u}}) := (\rho, \mathbf{m}^T, E_m, E_r)^T \in \mathbb{R}^s,$$

$$(A.10b) \quad \Theta : \mathbb{R}^s \ni \mathbf{u} := (\rho, \mathbf{m}^T, E_m, E_r)^T \mapsto \Theta(\mathbf{u}) := (\rho, \mathbf{m}^T, E_m, E_r, \Gamma(\mathbf{u}))^T \in \mathbb{R}^{\widehat{s}}.$$

$$\text{with } \Gamma(\mathbf{u}) := \rho + p(\mathbf{u}) \frac{1 - b\rho}{e(\mathbf{u})}.$$

Then, given $\hat{\mathbf{u}} := (\rho, \mathbf{m}^\top, E_m, E_r, \Gamma)^\top$, we define the extended flux

$$(A.11) \quad \hat{\mathbf{g}}(\hat{\mathbf{u}}) := \begin{pmatrix} v\rho \\ \mathbf{v} \otimes \mathbf{m} + \hat{p}(\hat{\mathbf{u}})\mathbb{I}_d \\ \mathbf{v}(E_m + \hat{p}(\hat{\mathbf{u}})) \\ vE_r \\ v\Gamma \end{pmatrix}, \quad \text{with} \quad \hat{p}(\hat{\mathbf{u}}) := \frac{(\Gamma - \rho)}{1 - b\rho} e(\Pi(\hat{\mathbf{u}})).$$

LEMMA A.4. *The operators Π , Θ , and $\hat{\mathbf{g}}$ satisfy the assumptions (A.6).*

Proof. Let us verify that (A.6a) holds. Let $\mathbf{u} := (\rho, \mathbf{m}, E_m, E_r)^\top \in \mathbb{R}^s$. Then

$$\Pi(\Theta(\mathbf{u})) = \Pi((\rho, \mathbf{m}, E_m, E_r, \Gamma(\mathbf{u}))^\top) = (\rho, \mathbf{m}, E_m, E_r)^\top = \mathbf{u}.$$

Let us now verify that (A.6b) holds. Let $\mathbf{u} := (\rho, \mathbf{m}, E_m, E_r)^\top$ be an arbitrary state in $\mathcal{B}(b)$. Then we observe that

$$\hat{p}(\Theta(\mathbf{u})) = \frac{(\Gamma(\mathbf{u}) - \rho)}{1 - b\rho} e(\Pi(\Theta(\mathbf{u}))) = \frac{p(\mathbf{u})}{e(\mathbf{u})} e(\mathbf{u}) = p(\mathbf{u}).$$

This gives $\hat{\mathbf{g}}(\Theta(\mathbf{u})) := (\mathbf{v}^\top \rho, \mathbf{v} \otimes \mathbf{m} + p(\mathbf{u})\mathbb{I}_d, \mathbf{v}^\top (E_m + p(\mathbf{u})), \mathbf{v}^\top E_r, \mathbf{v}^\top \Gamma(\mathbf{u}))^\top$, and the identity (A.6b) readily follows. \square

LEMMA A.5 (Existence&uniqueness). *For all pairs of states $(\mathbf{u}_L, \mathbf{u}_R)$ in $\mathcal{A}(b)$, the extended Riemann problem (A.7) has a unique self-similar solution \mathbf{v} that is entropic in the sense of Lax (see [27, §7]), and $\mathcal{A}(b)$ is invariant for $\Pi(\mathbf{v})$*

Proof. The construction of the solution is essentially the same as §4 in [9] with the exception that now the extended state contains the radiation energy.

Let us start by verifying that the states $\Theta(\mathbf{u}_L), \Theta(\mathbf{u}_R)$ are admissible to be able to use this construction. Let Z be in the index set $\{L, R\}$. By definition we have $\hat{\mathbf{u}}_Z := \Theta(\mathbf{u}_Z) := (\rho_Z, \mathbf{m}_Z, (E_m)_Z, (E_r)_Z, \Gamma(\mathbf{u}_Z))^\top$. As $\mathbf{u}_Z \in \mathcal{A}(b)$, we have $e(\mathbf{u}_Z) > 0$, and owing to the assumption (2.5), the tuple $(\rho_Z, \mathbf{m}_Z, (E_m)_Z, \Gamma(\mathbf{u}_Z))^\top$ is such that $\Gamma_Z := \Gamma(\mathbf{u}_Z) > 1$. Notice that the radiation energy is a passive scalar (i.e., $\partial_t E_r + (\mathbf{u} \cdot \mathbf{n}) \partial_x E_r = 0$); hence, the radiation energy stays constant on each side of the contact wave, and it is therefore necessarily positive since $\mathbf{u}_Z \in \mathcal{A}(b)$. As E_r is just a passive scalar in the Riemann problem and it is not coupled with the other components of the Riemann solution, we can apply the theory explained in §4 in [9] to construct a unique self-similar solution \mathbf{v} that is entropic in the sense of Lax. This solution satisfies $\Pi(\mathbf{v}) \in \mathcal{B}(b)$. \square

COROLLARY A.6 (Bar states). *For all $(\mathbf{u}_L, \mathbf{u}_R)$ in $\mathcal{A}(b)$ and all unit vector \mathbf{n} in \mathbb{R}^d , let $\hat{\lambda}_{\max}(\mathbf{n}, \mathbf{u}_L, \mathbf{u}_R)$ be any upper bound on the maximum wave speed in the extended Riemann problem (A.7). Let $\bar{\mathbf{u}}_{LR}(\lambda)$ be the bar state defined in (A.1). Then $\bar{\mathbf{u}}_{LR}(\lambda) \in \mathcal{A}(b)$ for all $\lambda \geq \hat{\lambda}_{\max}(\mathbf{n}, \mathbf{u}_L, \mathbf{u}_R)$.*

Note that the definition of the extended pressure in (A.11) makes the extended Riemann problem (A.7) easy to solve for any pressure oracle satisfying (2.5). The oracle is only invoked to compute the two pressures p_L and p_R . On the left of the contact wave, the ratio $\gamma := \frac{\Gamma}{\rho}$ is constant and equal to $\gamma_L := 1 + p_L \frac{1-b\rho_L}{\rho_L e_L}$, the extended pressure is equal to $(\gamma_L - 1) \frac{\rho e(\Pi \hat{\mathbf{u}})}{1-b\rho}$. On the right of the contact wave, the ratio $\gamma := \frac{\Gamma}{\rho}$ is also constant and equal to $\gamma_R := 1 + p_R \frac{1-b\rho_R}{\rho_R e_R}$, the extended pressure is equal to $(\gamma_R - 1) \frac{\rho e(\Pi \hat{\mathbf{u}})}{1-b\rho}$. A source code providing the upper bound $\hat{\lambda}_{\max}(\mathbf{n}, \mathbf{u}_L, \mathbf{u}_R)$ is publicly available at Clayton et al. [8].

Appendix B. Second Riemann problem. We study the Riemann problem associated with the hyperbolic system (3.6) and derive an upper bound on the maximum wave speed for this Riemann problem. The main result of this section is Lemma B.1.

B.1. Formulation of the problem. Let \mathbf{n} be a unit vector in \mathbb{R}^d . Let $\mathbf{u}_L := (\varrho_L, \mathbf{m}_L^\top, \mathbf{E}_{\mathbf{m},L}, \mathbf{E}_{\mathbf{r},L})^\top$ and $\mathbf{u}_R := (\varrho_R, \mathbf{m}_R^\top, \mathbf{E}_{\mathbf{m},R}, \mathbf{E}_{\mathbf{r},R})^\top$ be given left and right states. Let us set $v_L := \mathbf{v}_L \cdot \mathbf{n}$, and $E_L := \mathbf{E}_{\mathbf{r},L} + \frac{1}{2}\rho_L v_L^2$. Similarly we define $v_R := \mathbf{v}_R \cdot \mathbf{n}$, and $E_R := \mathbf{E}_{\mathbf{r},R} + \frac{1}{2}\rho_R v_R^2$. Then, the Riemann problem associated with the hyperbolic system (3.6) reduces to solving

$$(B.1a) \quad \partial_t \rho = 0$$

$$(B.1b) \quad \partial_t(\rho v) + \partial_x p_r = 0, \quad p_r := \frac{1}{3}(E - \frac{\rho}{2}v^2),$$

$$(B.1c) \quad \partial_t E + \partial_x(v p_r) = 0,$$

with left and right states $(\varrho_L, \mathbf{v}_L, \mathbf{E}_L)^\top$ and $(\varrho_R, \mathbf{v}_R, \mathbf{E}_R)^\top$, respectively. Using the change of variables $(\mathbf{v}, E)^\top \mapsto (v, E_r := E - \frac{\rho}{2}v^2)^\top$, the nontrivial part of the above system can be rewritten in the following form for which the computation of the eigenvalues of the Jacobian matrix of the flux is easier

$$\partial_t \begin{pmatrix} v \\ E_r \end{pmatrix} = -\frac{1}{3} \begin{pmatrix} \frac{1}{\rho} \partial_x E_r \\ E_r \partial_x v \end{pmatrix} = -\frac{1}{3} \begin{pmatrix} 0 & \frac{1}{\rho} \\ E_r & 0 \end{pmatrix} \partial_x \begin{pmatrix} v \\ E_r \end{pmatrix}.$$

The eigenvalues of the Jacobian matrix are $\pm \frac{1}{3}\sqrt{E_r/\rho}$. Hence, the system (B.1) is hyperbolic; the three eigenvalues are $-\frac{1}{3}\sqrt{E_r/\rho}$, 0, and $\frac{1}{3}\sqrt{E_r/\rho}$. The eigenvalues $-\frac{1}{3}\sqrt{E_r/\rho}$ and $\frac{1}{3}\sqrt{E_r/\rho}$ are genuinely nonlinear. The eigenvalue 0 is linearly degenerate and is associated with a contact wave.

B.2. Rarefaction wave. We first construct the rarefaction solution associated with the left wave. Recall that the density is equal to ρ_L in the left wave. Let $\xi := x/t$ be the self-similarity variable. Let us abuse the notation and let us denote $v(\xi)$ the velocity and $p(\xi)$ the pressure. The momentum conservation equation reduces to $-\xi \partial_\xi v + \rho_L^{-1} \partial_\xi p = 0$. Recalling that $E_r = 3p$, we have $\xi = -\sqrt{p/3\rho_L}$ in the left wave. The conservation equation is

$$(B.2) \quad \sqrt{\frac{\rho_L}{12}} \partial_\xi v + \frac{1}{2\sqrt{p}} \partial_\xi p = 0.$$

This implies that the dependency with respect to the pressure of the velocity and the wave speed in the left rarefaction wave is given by

$$(B.3) \quad v = -\sqrt{\frac{12}{\rho_L}} (\sqrt{p} - \sqrt{p_L}) + v_L, \quad \lambda_L(p) = -\sqrt{\frac{p}{3\rho_L}}.$$

Using the same argument, and recalling that the self-similar variable is $\xi = \sqrt{p/3\rho_R}$ in the right wave, we obtain that the dependency with respect to the pressure of the velocity and the wave speed in the right rarefaction wave is given by

$$(B.4) \quad v = \sqrt{\frac{12}{\rho_R}} (\sqrt{p} - \sqrt{p_R}) + v_R, \quad \lambda_R(p) = \sqrt{\frac{p}{3\rho_R}}.$$

B.3. Shock wave. If the left wave is a shock, the Rankine-Hugoniot relation implies that there exists $s < 0$ so that

$$(B.5) \quad s\rho_L(v - v_L) = p - p_L, \quad s(3p + \frac{1}{2}\rho_L v^2 - 3p_L - \frac{1}{2}\rho_L v_L^2) = vp - v_L p_L.$$

where used that $E = 3p + \frac{1}{2}\rho_L v^2$. Hence

$$\begin{aligned} (3p + \frac{1}{2}\rho_L v^2 - 3p_L - \frac{1}{2}\rho_L v_L^2)(p - p_L) &= \rho_L(vp - v_L p_L)(v - v_L) \\ &\implies \\ -\frac{1}{2}\rho_L(p + p_L)v^2 + \rho_L v_L(p_L + p)v + 3(p - p_L)^2 - \frac{1}{2}\rho_L v_L^2(p + p_L) &= 0. \end{aligned}$$

The discriminant of the quadratic equation in v is

$$\Delta := 6(p - p_L)^2 \rho_L(p + p_L).$$

Recalling that $s < 0$ and the pressure increases along the shock curve (i.e., $p \geq p_L$), we conclude from (B.5) that the solution to the quadratic equation must be such that $v - v_L \leq 0$; hence, the velocity and the wave speed in left shock solution are given by

$$v = v_L - \sqrt{\frac{6}{\rho_L} \frac{(p - p_L)}{\sqrt{p + p_L}}}, \quad \lambda_L(p) = -\sqrt{\frac{p + p_L}{6\rho_L}}.$$

Similarly, the shock solution in the right wave is given by

$$v = v_R + \sqrt{\frac{6}{\rho_R} \frac{(p - p_R)}{\sqrt{p + p_R}}}, \quad \lambda_R(p) = \sqrt{\frac{p + p_R}{6\rho_R}}.$$

B.4. Description of the solution. We define the index set $\{L, R\}$, and for all Z in the index set $\{L, R\}$ we define the function $f_Z : \mathbb{R}_{\geq 0} \rightarrow \mathbb{R}$

$$(B.6) \quad f_Z(p) = \begin{cases} \sqrt{\frac{6}{\rho_Z} \frac{(p - p_Z)}{\sqrt{p + p_Z}}} & \text{if } p_Z \leq p \text{ (shock),} \\ \sqrt{\frac{12}{\rho_Z} (\sqrt{p} - \sqrt{p_Z})} & \text{if } p \leq p_Z \text{ (expansion).} \end{cases}$$

This definition implies that the velocity in the left wave is given by $v = -f_L(p) + v_L$ and the velocity in the right wave is given by $v = f_R(p) + v_R$. The left and right waves can be continuously reconnected only if there exists $p^* \geq 0$ so that $f_R(p^*) + v_R = -f_L(p^*) + v_L$. We thus define $\phi(p) = f_R(p) + f_L(p) + v_R - v_L$ for all $p \geq 0$. The function ϕ is monotone strictly increasing. Hence, the pressure p^* connecting the left and right waves solves the nonlinear equation $\phi(p^*) = 0$. Once p^* is found, the extreme wave speed of the left and right waves are

$$(B.7) \quad \lambda_L^- = -\sqrt{\frac{p_L + \max(p^*, p_L)}{6\rho_L}}, \quad \lambda_R^+ = \sqrt{\frac{p_R + \max(p^*, p_R)}{6\rho_R}}.$$

We finish this section by showing how p^* can be estimated from above.

B.4.1. Case 0: Vacuum, $p^* = 0$. If $\phi(0) > 0$, then the equation $\phi(p) = 0$ has no root. This means that vacuum forms between the left and the right waves. Vacuum forms when

$$(B.8) \quad v_R - v_L - \sqrt{\frac{12p_L}{\rho_L}} - \sqrt{\frac{12p_R}{\rho_R}} > 0.$$

In this case we conventionally set $p^* = 0$. Note that if $\phi(0) = 0$, then $p^* = 0$ is the unique solution. The left and right waves are both expansions.

B.4.2. Case 1: $0 < p^*$ and $0 < \phi(p_{\min})$. Let us denote $p_{\min} := \min(p_L, p_R)$. The condition $0 < \phi(p_{\min})$ implies that the left and the right waves are both expansions (since $p^* < p_{\min}$), and we have

$$(B.9) \quad p^* = \left(\frac{v_L - v_R + \sqrt{\frac{12p_L}{\rho_L}} + \sqrt{\frac{12p_R}{\rho_R}}}{\sqrt{\frac{12}{\rho_L}} + \sqrt{\frac{12}{\rho_R}}} \right)^2.$$

B.4.3. Case 2: $\phi(p_{\min}) < 0 < \phi(p_{\max})$. Let us denote $p_{\min} := \min(p_L, p_R)$ and $p_{\max} := \max(p_L, p_R)$. The solution is composed of an expansion and a shock when $\phi(p_{\min}) < 0 < \phi(p_{\max})$. The root of $\phi(p) = 0$ can be computed by using verbatim Algorithm 2 from [16]. The algorithm can be initialized by using p_{\min} and p_{\max} as lower and upper bounds on p^* , respectively.

B.4.4. Case 3: $\phi(p_{\max}) < 0$. The solution is composed of two shocks when $\phi(p_{\max}) < 0$. That is,

$$\phi(p) = \sqrt{\frac{6}{\rho_L}} \frac{p - p_L}{\sqrt{p + p_L}} + \sqrt{\frac{6}{\rho_R}} \frac{p - p_R}{\sqrt{p + p_R}} + v_R - v_L.$$

Note that an upper bound on p^* can be obtained by computing the zero of the following function:

$$\tilde{\phi}(p) := \sqrt{\frac{3}{\rho_L}} \frac{p - p_L}{\sqrt{p}} + \sqrt{\frac{3}{\rho_R}} \frac{p - p_R}{\sqrt{p}} + v_R - v_L,$$

since $\phi(p) > \tilde{\phi}(p)$ for all $p > p_{\max}$. The unique zero of $\tilde{\phi}(p) = 0$ is obtained by making the substitution $\sqrt{p} \rightarrow x$ and solving the quadratic equation $ax^2 + bx + c = 0$ with

$$a := \sqrt{\frac{3}{\rho_L}} + \sqrt{\frac{3}{\rho_R}}, \quad b := v_R - v_L, \quad c := -\sqrt{\frac{3}{\rho_L}} p_L - \sqrt{\frac{3}{\rho_R}} p_R.$$

Letting x_+ be the largest root of the quadratic equation, and setting $\tilde{p}^* := x_+^2$, we necessarily have $p^* < \tilde{p}^*$. Then, the zero of ϕ can be computed by using verbatim Algorithm 2 from [16] and initializing the algorithm with p_{\max} as lower bound and \tilde{p}^* as upper bound.

B.5. Conclusion. The main result of this section is the following result.

LEMMA B.1 (Wave speed upper bound). *With p^* defined above and the definitions (B.7), a guaranteed upper bound on the maximum wave speed in the Riemann problem (B.1) is given by*

$$(B.10) \quad \hat{\lambda}_{\max}(\mathbf{n}, \mathbf{w}_L, \mathbf{w}_R) = \max(-\lambda_L^-(p^*), \lambda_R^+(p^*)).$$

References.

- [1] D. Arndt, W. Bangerth, M. Bergbauer, M. Feder, M. Fehling, J. Heinz, T. Heister, L. Heltai, M. Kronbichler, M. Maier, P. Munch, J.-P. Pelteret, B. Turcksin, D. Wells, and S. Zampini. The `deal.II` library, version 9.5. *Journal of Numerical Mathematics*, 31(3):231–246, 2023.
- [2] C. Baldwin, P. N. Brown, R. Falgout, F. Graziani, and J. Jones. Iterative linear solvers in a 2d radiation–hydrodynamics code: methods and performance. *Journal of Computational Physics*, 154(1):1–40, 1999.

- [3] J. Bates, D. Knoll, W. Rider, R. B. Lowrie, and V. Mousseau. On consistent time-integration methods for radiation hydrodynamics in the equilibrium diffusion limit: low-energy-density regime. *Journal of Computational Physics*, 167(1):99–130, 2001.
- [4] S. Bolding, J. Hansel, J. D. Edwards, J. E. Morel, and R. B. Lowrie. Second-order discretization in space and time for radiation-hydrodynamics. *J. Comput. Phys.*, 338:511–526, 2017. doi: 10.1016/j.jcp.2017.02.063. URL <https://doi.org/10.1016/j.jcp.2017.02.063>.
- [5] C. Buet and B. Despres. Asymptotic analysis of fluid models for the coupling of radiation and hydrodynamics. *Journal of Quantitative Spectroscopy and Radiative Transfer*, 85(3-4):385–418, 2004.
- [6] C. Buet and B. Despres. Asymptotic preserving and positive schemes for radiation hydrodynamics. *J. Comput. Phys.*, 215(2):717–740, 2006. ISSN 0021-9991. doi: 10.1016/j.jcp.2005.11.011. URL <https://doi.org/10.1016/j.jcp.2005.11.011>.
- [7] B. Clayton and E. J. Tovar. Preserving the minimum principle on the entropy for the compressible euler equations with general equations of state, 2025. URL <https://arxiv.org/abs/2503.10612>.
- [8] B. Clayton, J.-L. Guermond, and B. Popov. Upper bound on the maximum wave speed in Riemann problems for the Euler equations with tabulated equation of state, apr 2021. URL <https://doi.org/10.5281/zenodo.4685868>. This code is described in the paper "Invariant domain preserving approximations for the Euler equations with tabulated equation of state".
- [9] B. Clayton, J.-L. Guermond, and B. Popov. Invariant domain-preserving approximations for the Euler equations with tabulated equation of state. *SIAM J. Sci. Comput.*, 44(1):A444–A470, 2022. ISSN 1064-8275. doi: 10.1137/21M1414097. URL <https://doi.org/10.1137/21M1414097>.
- [10] W. Dai and P. R. Woodward. Numerical simulations for radiation hydrodynamics. i. diffusion limit. *Journal of Computational Physics*, 142(1):182–207, 1998.
- [11] T. A. Dao, M. Nazarov, and I. Tomas. A structure preserving numerical method for the ideal compressible MHD system. *J. Comput. Phys.*, 508:Paper No. 113009, 25, 2024. ISSN 0021-9991. doi: 10.1016/j.jcp.2024.113009. URL <https://doi.org/10.1016/j.jcp.2024.113009>.
- [12] M. O. Delchini, J. C. Ragusa, and J. Morel. Entropy-based artificial viscosity stabilization for non-equilibrium grey radiation-hydrodynamics. *Journal of Computational Physics*, 296:293–313, 2015.
- [13] M. O. Delchini, J. C. Ragusa, and J. Ferguson. Viscous regularization of the full set of nonequilibrium-diffusion grey radiation-hydrodynamic equations. *Internat. J. Numer. Methods Fluids*, 85(1):30–47, 2017. ISSN 0271-2091. doi: 10.1002/fld.4371. URL <https://doi.org/10.1002/fld.4371>.
- [14] A. Ern and J.-L. Guermond. *Finite elements II—Galerkin approximation, elliptic and mixed PDEs*, volume 73 of *Texts in Applied Mathematics*. Springer, Cham, 2021. ISBN 978-3-030-56922-8; 978-3-030-56923-5. doi: 10.1007/978-3-030-56923-5. URL <https://doi.org/10.1007/978-3-030-56923-5>.
- [15] J. M. Ferguson, J. E. Morel, and R. Lowrie. The equilibrium-diffusion limit for radiation hydrodynamics. *Journal of Quantitative Spectroscopy and Radiative Transfer*, 202:176–186, 2017.
- [16] J.-L. Guermond and B. Popov. Fast estimation from above of the maximum wave speed in the riemann problem for the euler equations. *Journal of Computational Physics*, 321:908–926, 2016. ISSN 0021-9991. doi: <https://doi.org/10.1016/j.jcp.2016.05.054>. URL <https://www.sciencedirect.com/science/article/>

pii/S0021999116301991.

[17] J.-L. Guermond and B. Popov. Invariant domains and first-order continuous finite element approximation for hyperbolic systems. *SIAM J. Numer. Analysis*, 54(4):2466–2489, 2016. doi: 10.1137/16M1074291. URL <http://dx.doi.org/10.1137/16M1074291>.

[18] J.-L. Guermond, B. Popov, and I. Tomas. Invariant domain preserving discretization-independent schemes and convex limiting for hyperbolic systems. *Comput. Methods Appl. Mech. Engrg.*, 347:143–175, 2019. doi: 10.1016/j.cma.2018.11.036. URL <https://doi.org/10.1016/j.cma.2018.11.036>.

[19] J.-L. Guermond, M. Kronbichler, M. Maier, B. Popov, and I. Tomas. On the implementation of a robust and efficient finite element-based parallel solver for the compressible Navier-Stokes equations. *Computer Methods in Applied Mechanics and Engineering*, 389:114250, 2022.

[20] J.-L. Guermond, B. Popov, L. Saavedra, and M. Sheridan. Invariant-domain preserving and locally mass conservative approximation of the lagrangian hydrodynamics equations. *Computer Methods in Applied Mechanics and Engineering*, 441:117927, 2025. ISSN 0045-7825. doi: <https://doi.org/10.1016/j.cma.2025.117927>. URL <https://www.sciencedirect.com/science/article/pii/S0045782525001999>.

[21] A. Harten, P. D. Lax, and B. van Leer. On upstream differencing and Godunov-type schemes for hyperbolic conservation laws. *SIAM Rev.*, 25(1):35–61, 1983. ISSN 0036-1445. doi: 10.1137/1025002. URL <https://doi.org/10.1137/1025002>.

[22] C.-C. He, B. D. Wibking, and M. R. Krumholz. An asymptotically correct implicit-explicit time integration scheme for finite volume radiation-hydrodynamics. *Monthly Notices of the Royal Astronomical Society*, 531(1):1228–1242, 05 2024. ISSN 0035-8711. doi: 10.1093/mnras/stae1244. URL <https://doi.org/10.1093/mnras/stae1244>.

[23] D. Knoll, W. Rider, and G. Olson. An efficient nonlinear solution method for non-equilibrium radiation diffusion. *Journal of Quantitative Spectroscopy and Radiative Transfer*, 63(1):15–29, 1999. ISSN 0022-4073. doi: [https://doi.org/10.1016/S0022-4073\(98\)00132-0](https://doi.org/10.1016/S0022-4073(98)00132-0). URL <https://www.sciencedirect.com/science/article/pii/S0022407398001320>.

[24] D. Knoll, L. Chacon, L. Margolin, and V. Mousseau. On balanced approximations for time integration of multiple time scale systems. *Journal of Computational Physics*, 185(2):583–611, 2003. ISSN 0021-9991. doi: [https://doi.org/10.1016/S0021-9991\(03\)00008-1](https://doi.org/10.1016/S0021-9991(03)00008-1). URL <https://www.sciencedirect.com/science/article/pii/S0021999103000081>.

[25] L. A. N. Laboratory. Exactpack: An open-source software package for code verification, 2025. URL <https://github.com/lanl/ExactPack>.

[26] E. W. Larsen, A. Kumar, and J. E. Morel. Properties of the implicitly time-differenced equations of thermal radiation transport. *Journal of Computational Physics*, 238:82–96, 2013. ISSN 0021-9991. doi: <https://doi.org/10.1016/j.jcp.2012.11.034>. URL <https://www.sciencedirect.com/science/article/pii/S0021999112007140>.

[27] P. D. Lax. Hyperbolic systems of conservation laws. II. *Comm. Pure Appl. Math.*, 10:537–566, 1957. ISSN 0010-3640.

[28] R. B. Lowrie and J. D. Edwards. Radiative shock solutions with grey nonequilibrium diffusion. *Shock waves*, 18(2):129–143, 2008. doi: <https://doi.org/10.1007/s00193-008-0143-0>.

[29] R. B. Lowrie, J. Morel, and J. Hittinger. The coupling of radiation and hydro-

dynamics. *The astrophysical journal*, 521(1):432, 1999.

- [30] M. Maier and M. Kronbichler. Efficient parallel 3D computation of the compressible Euler equations with an invariant-domain preserving second-order finite-element scheme. *ACM Transactions on Parallel Computing*, 8(3):16:1–30, 2021.
- [31] D. Mihalas and B. W. Mihalas. *Foundations of radiation hydrodynamics*. Courier Corporation, 2013.
- [32] H. Nessyahu and E. Tadmor. Nonoscillatory central differencing for hyperbolic conservation laws. *J. Comput. Phys.*, 87(2):408–463, 1990. ISSN 0021-9991. doi: 10.1016/0021-9991(90)90260-8. URL [https://doi.org/10.1016/0021-9991\(90\)90260-8](https://doi.org/10.1016/0021-9991(90)90260-8).
- [33] R. E. Olson, R. J. Leeper, J. L. Kline, A. B. Zylstra, S. A. Yi, J. Biener, T. Braun, B. J. Kozioziemski, J. D. Sater, P. A. Bradley, R. R. Peterson, B. M. Haines, L. Yin, L. F. Berzak Hopkins, N. B. Meezan, C. Walters, M. M. Biener, C. Kong, J. W. Crippen, G. A. Kyrala, R. C. Shah, H. W. Herrmann, D. C. Wilson, A. V. Hamza, A. Nikroo, and S. H. Batha. First liquid layer inertial confinement fusion implosions at the national ignition facility. *Phys. Rev. Lett.*, 117:245001, Dec 2016. doi: 10.1103/PhysRevLett.117.245001. URL <https://link.aps.org/doi/10.1103/PhysRevLett.117.245001>.
- [34] G. Pomraning. The non-equilibrium marshak wave problem. *Journal of Quantitative Spectroscopy and Radiative Transfer*, 21(3):249–261, 1979. ISSN 0022-4073. doi: [https://doi.org/10.1016/0022-4073\(79\)90016-5](https://doi.org/10.1016/0022-4073(79)90016-5). URL <https://www.sciencedirect.com/science/article/pii/0022407379900165>.
- [35] Z. Sheng, J. Yue, and G. Yuan. Monotone finite volume schemes of nonequilibrium radiation diffusion equations on distorted meshes. *SIAM Journal on Scientific Computing*, 31(4):2915–2934, 2009.
- [36] B. S. Southworth, H. Park, S. Tokareva, and M. Charest. Implicit-explicit runge-kutta for radiation hydrodynamics i: Gray diffusion. *Journal of Computational Physics*, 518:113339, 2024.
- [37] J. Thrussell and J. M. Ferguson. Exactpack: A python library of exact analytic solutions. *SoftwareX*, 24, 10 2023. doi: 10.1016/j.softx.2023.101560. URL <https://www.osti.gov/biblio/2204208>.
- [38] S. Zheng, M. Tang, Q. Zhang, and T. Xiong. High order conservative ldg-imex methods for the degenerate nonlinear non-equilibrium radiation diffusion problems. *Journal of Computational Physics*, 503:112838, 2024.